

**INVESTIGATING THE EFFECTIVENESS OF DISTRIBUTED  
ELECTRIC PROPULSION FOR AIRCRAFTS**

**Chingiz Arystanbekov, BEng**

**Submitted in fulfillment of the requirements  
for the degree of Master of Science  
in Mechanical & Aerospace Engineering**



**NAZARBAYEV  
UNIVERSITY**

**School of Engineering and Digital Sciences  
Department of Mechanical & Aerospace Engineering  
Nazarbayev University**

53 Kabanbay Batyr Avenue,  
Astana city, Kazakhstan, 010000

**Supervisor:** Associate Professor Basman Elhadidi

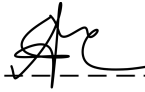
**Co-supervisor:** Professor Essam Shehab

**April 2023**

## DECLARATION

I hereby, declare that this manuscript, entitled “*Investigating the Effectiveness of Distributed Electric Propulsion for aircrafts*”, is the result of my own work except for quotations and citations, which have been duly acknowledged.

I also declare that, to the best of my knowledge and belief, it has not been previously or concurrently submitted, in whole or in part, for any other degree or diploma at Nazarbayev University or any other national or intentional institution.

----------

Name: Chingiz Arystanbekov

Date: 7.04.2023

## Abstract

This work presents an experimental evaluation of the performance of a two-propeller propulsion system. Various propeller placement configurations relative to the trailing edge were investigated. The aerodynamic performance of a wing with two propellers was compared to that of a baseline wing using a NACA 2418 airfoil. The experimental work was conducted in a 600 mm wide AF1600s subsonic wind tunnel at  $Re = 91,000$ . The results of the first experiment indicate that propeller placement plays a crucial role in determining the vertical force generated by a model aircraft, especially at different throttle settings. Specifically, the configuration with propellers located at  $x/c = 1/3$  and  $y/c = 0.71$  yielded the highest vertical force at 20% throttle, while the configuration with propellers closer to the trailing edge ( $x/c = 1/9$ ) resulted in the greatest vertical force at 40% throttle. The net vertical force acting on the wing was found to be increased by 15.2% and 34.12% at 20% and 40% throttle, respectively, compared to the clear wing.

To isolate the impact of the propellers on the wing the thrust generated by the propellers was measured and later accounted for in the analysis. This approach enabled the evaluation the aero-coupling effect of the propellers on the wing. The findings of the first experiment were inconclusive, as the lift coefficient initially increased up to an angle of attack (AOA) of  $10^\circ$ , then slightly dropped before increasing again. This behavior may suggest a stall delay, but additional research using particle image velocimetry (PIV) is needed to confirm this hypothesis.

To achieve steady level characteristics, the second experiment was performed by adjusting the throttle settings and free stream velocity at various angles of attack ranging from  $2^\circ$  to  $20^\circ$ . The objective was to ensure that the net vertical and horizontal forces were equal to zero. The findings indicated that the minimum required throttle and free stream velocity were 26.5% and 11.42 m/s, respectively, which were observed at an angle of attack of  $10^\circ$ .

The findings of this study highlight the importance of propeller placement in determining the net forces acting on a wing. Firstly, placing the propellers too close to the wing may result in a degradation of overall performance. Secondly, positioning the propellers vertically above the trailing edge is effective at smaller angles of attack, as it accelerates the flow above the wing, contributing to the lift. Furthermore, the research indicates that adjustments in throttle settings and free stream velocity can help achieve steady level flight characteristics.

## Acknowledgements

Firstly, I would like to express my sincere thanks to Professor Basman Elhadidi for his invaluable guidance, persistent encouragement, and unwavering dedication to my thesis project. His expertise, feedback, and support have been critical in shaping my research and enhancing its quality. I am deeply appreciative of Professor Essam Shehab, whose weekly meetings provided me with vital insights and perspectives related to my thesis. His constructive feedback and suggestions have been invaluable in refining my research methodology and analysis. Additionally, I express my gratitude to Professor Didier Talamona for generously providing me with a 3D printer and the necessary plastic materials to support my experimental work.

Finally, I want to express my deep appreciation to my parents and my friend Erkenaz for their consistent support and encouragement during my academic journey. Their enduring love and motivation played a crucial role in helping me overcome obstacles and accomplish my goals.

# Table of Contents

Abstract .....	3
Acknowledgements .....	4
Table of Contents .....	5
List of Figures .....	7
List of Tables.....	9
Nomenclature .....	10
<b>Chapter 1 – Introduction .....</b>	<b>11</b>
1.1 Background .....	11
1.2 Literature Review .....	13
1.2.1 Aerodynamic Effects: Stall.....	13
1.2.2 Aerodynamic Effects: BLI.....	14
1.2.3 Propeller/Wing Interaction .....	14
1.2.3 DEP: Numerical Studies .....	16
1.2.4 DEP: Experimental studies .....	19
1.3 Summary of the Literature & Research Gaps .....	21
1.4 Research Aim and Objectives .....	22
<b>Chapter 2 – Experimental Setup.....</b>	<b>23</b>
2.1 Introduction .....	23
2.2 Design description .....	23
2.2.1 Baseline wing.....	23
2.2.2 Propeller characteristics.....	24
2.2.3 Brushless Motor .....	24
2.2.4 Wind Tunnel .....	25
2.2.5 DEP Configuration.....	26
2.3 Measurement process description.....	26
2.3.1 Angle of Attack.....	26
2.3.2 Freestream Velocity & Pressure.....	27
2.3.3 Lift and Drag.....	28
2.3.4 Propeller RPM.....	28
2.4 Experiment procedure.....	29
2.4.1 Experiment #1: Effect on Net Forces .....	29
3.4.2 Experiment #1: Effect on Lift & Drag .....	33
3.4.3 Experiment #2: Steady Level Flight.....	34

Chapter 3 – Results & Discussion .....	38
4.1 Experiment 1: Propeller Position Effect on Net Forces .....	38
4.1.1 Net Vertical Force .....	38
4.1.2 Net Horizontal Force .....	42
4.2 Experiment 1: Effect on Lift & Drag .....	44
4.3 Experiment 2: Steady Level Flight .....	48
Chapter 4 – Conclusion & Future Work .....	52
4.1 Conclusion .....	52
4.2 Limitations .....	53
4.3 Future Work .....	53
References .....	55
Appendix A .....	59

## List of Figures

<b>Figure 1.1</b> STOL aircraft examples [11, 12].....	12
<b>Figure 1.2</b> AIRBUS eVTOL aircraft Vahana [14].....	13
<b>Figure 1.3</b> Variation in lift-coefficient with angle of attack for an airfoil [15] .....	14
<b>Figure 1.4</b> The wing's exposure to propeller flow [17] .....	15
<b>Figure 1.5</b> Piaggio P.180 Avanti; pusher configuration aircraft [20] .....	16
<b>Figure 1.6</b> Propeller and Actuator disk [25] .....	17
<b>Figure 1.7</b> Lift distribution along the span [26] .....	18
<b>Figure 1.8</b> Lift-to-drag ratio at different angles of attack and propeller positions [27] .....	18
<b>Figure 1.9</b> Lift coefficient at 15 and 20 m/s [29] .....	19
<b>Figure 1.10</b> Lift and Drag vs AOA at different throttle [30] .....	20
<b>Figure 1.11</b> Cl vs AOA [33] .....	21
<b>Figure 2.1</b> Baseline Wing .....	24
<b>Figure 2.2</b> 5040 Propeller .....	24
<b>Figure 2.3</b> Brushless Motor .....	25
<b>Figure 2.4</b> Wind tunnel schematics .....	25
<b>Figure 2.5</b> CAD model of DEP .....	26
<b>Figure 2.6</b> Balance Angle Feedback .....	27
<b>Figure 2.7</b> Pressure measuring device .....	27
<b>Figure 2.8</b> Three-Component Balance .....	28
<b>Figure 2.9</b> Arduino board .....	29
<b>Figure 2.10</b> Four configurations .....	30
<b>Figure 2.11</b> Experiment #1 flowchart .....	32
<b>Figure 2.12</b> TYTORBOTICS 1580 .....	33
<b>Figure 2.13</b> Forces acting on the wing .....	34
<b>Figure 2.14</b> Fourth Configuration .....	35
<b>Figure 2.15</b> Experiment #2 flowchart .....	37
<b>Figure 3.1</b> Net Vertical Force in each Position.....	40
<b>Figure 3.2</b> Net vertical force at 20% throttle .....	40
<b>Figure 3.3</b> Net vertical force at 40% throttle .....	41
<b>Figure 3.4</b> Net Horizontal Force in each Position.....	43
<b>Figure 3.5</b> Net horizontal force .....	44
<b>Figure 3.6</b> Lift Coefficient in each Position .....	45

<b>Figure 3.7</b> Drag Coefficient in each Position .....	46
<b>Figure 3.8</b> Diagram of flow at 0° AOA (1 <sup>st</sup> and 3 <sup>rd</sup> configurations, respectively) .....	46
<b>Figure 3.9</b> Diagram of flow at higher AOA (1 <sup>st</sup> configurations) .....	47
<b>Figure 3.10</b> Free body Diagram .....	48
<b>Figure 3.11</b> Throttle vs AOA.....	49
<b>Figure 3.12</b> Velocity vs AOA .....	49



## List of Tables

Table 2.1 Wing dimension .....	24
Table 2.2 Operating conditions.....	26
Table 2.3 Configurations .....	29
Table 2.4 Variables 1 .....	31
Table 2.5 Variables 2 .....	36
Table 3.1 Net Vertical & Net horizontal forces at $\alpha = 10^\circ$ .....	39
Table 3.2 Trimmed parameters.....	48

# Nomenclature

## Abbreviations

AOA	Angle of Attack
AR	Aspect Ratio
CFD	Computational Fluid Dynamics
DEP	Distributed Electric Propulsion
DP	Distributed Propulsion
ESC	Electronic Speed Controller
eVTOL	Electric Vertical Takeoff and Landing
NACA	National Advisory Committee for Aeronautics
NASA	National Aeronautics and Space Administration
Re	Reynolds Number
RPM	Revolutions per Minute
STOL	Short Takeoff and Landing
UAM	Urban Air Mobility
UAV	Urban Air Vehicles
VTOL	Vertical Takeoff and Landing

## Greek symbols

$\alpha$	angle of attack
$\rho$	density

## Roman Symbols

A	Wing surface area
B	Wingspan
$C_D$	Drag coefficient
$C_L$	Lift coefficient
d	Propeller diameter
$F_x$	Net Force along X-axis
$F_y$	Net Force along Y-axis
T	Thrust
$U_\infty$	Freestream velocity

# Chapter 1 – Introduction

---

*This chapter provides a brief introduction to the technology of Distributed Electric Propulsion. Several illustrative examples of eVTOL and STOL aircraft featuring DEP are also included.*

## 1.1 Background

Global warming is regarded as one of the most pressing problems humanity faces today. The use of fossil fuels as a source of energy for manufacturing, electricity and heating systems, agriculture, and transportation is one of the factors that contribute to global warming. Among all means of transportation, 12% of total CO<sub>2</sub> emissions are produced by airplanes [1]. According to the "net-zero emissions" goal of aerospace industries, this number is supposed to reach zero by 2050 [2]. Consequently, research is being conducted in four primary areas: (i) sustainable aviation biofuel, (ii) fuel consumption optimization, (iii) route optimization, and (iv) more efficient aircraft. Optimizing airframe design and using modern propulsion technology are two aspects of airplane efficiency research.

Airframe design optimization is the practice of seeking improved wing designs to enhance the aerodynamics of aircraft. NASA, Boeing, and Airbus are substantially investing in the blended-wing body concept, which is considered one of the most promising designs for cutting emissions. A blended-wing body is a form of fixed-wing aircraft in which the wing and fuselage are not clearly separated [3]. Nicolas Woyevodsky, who created the BWB theory and conducted wind tunnel research, constructed the first real model in 1924 [4]. However, none of the prototypes released prior to the 1990s were practical in terms of safety and dependability. Since then, NASA has conducted experimental tests on a variety of scaled aircraft, including the X-48 UAV and N3-X [5, 6]. It was determined that modern airplane models with blended wings can save up to 20% more fuel than older versions.

Installing more efficient propulsion systems is a second approach to building more efficient airplanes. In particular, research institutions are investigating in two directions: hybrid-electric and all-electric propulsion systems. Purely electric aircraft have a short flight range and can only carry a small number of passengers due to the additional weight from the batteries. Consequently, hybrid systems are now viewed as a compromise between emissions and practicality. As the use of electric aircraft in large-scale commercial aviation is not viable, this technology has emerged as a mode of urban transportation, increasing the value of Urban Air Mobility (UAM). As a result, the demand for aircraft with Short Takeoff and Landing (STOL) and Vertical Takeoff and Landing (VTOL) capabilities is growing. The demand can

be addressed by distributing the thrust along the whole span of the wing. In electric propulsion systems, the power sources are conveniently decoupled from the propellers, enabling greater flexibility in terms of propellers' quantity and arrangement along the wing. Introducing several propulsion units and distributing them over the span enhances aerodynamics of an aircraft, hence increasing the viability of electric aircraft [7]. Particularly, the addition of several propulsion units helps lessen vortices at the wingtips, hence reducing drag [8]. In addition, the propulsion elements positioned above the span accelerate the upper flow, delaying flow separation [9]. Eventually, the greater lift is achieved at greater angles of attack, which indicates stall delay. Additionally, DEP enables the exploration and analysis of many various configurations to improve aircraft efficiency [10]. For example, NASA created the X-57 Maxwell All-Electric Aircraft, which has 14 electric motors, 12 of which are only active during the ascent and descent phases of flight (Figure 1.1a) [11]. Multiple propulsion systems generate a wind-blowing effect that facilitates short takeoff and landing distances. During cruising, the small propellers are deactivated and only two propellers at the wingtips remain active to generate adequate thrust. This simple approach makes X-57 Maxwell highly efficient, as the propellers considerably minimize the wake-induced drag at the wingtips. However, current batteries are insufficient to allow the aircraft to fly for more than an hour. NASA anticipates that X-57 will be competitive soon as battery energy density grows.



(a) NASA X-57 Maxwell

(b) Scaled AMPERE by ONERA

**Figure 1.1** STOL aircraft examples [11, 12]

The French scientific organization ONERA initiated the AMPERE project in 2013 (Figure 1.1b) [12]. The maximum power output of the aircraft approached 400 kW. Forty propellers were powered by Li-ion batteries and fuel cells. To date, numerical simulations have been done and validated by wind tunnel experiments on a 1/5-scale model. Differential thrust generated by several fans can result in enhanced flight control, as stressed by the authors. Due

to funding constraints, the project was abandoned despite the satisfactory validation of the numerical model.

Both the X-57 Maxwell and AMPERE are classified short takeoff and landing (STOL) aircraft, developed particularly for use in urban environments. X-57 Maxwell was a more successful project in terms of idea execution because the model was based on the previously existing Tecnam P2006T baseline aircraft. In contrast, AMPERE was cancelled prior to any actual flight testing.

By positioning the propulsors at an angle to the horizon, vertical takeoff and landing can be achieved. The vertical takeoff and landing capabilities of eVTOL aircraft is comparable to that of helicopters, yet eVTOL aircraft differ from helicopters in several significant aspects, such as noise levels, maintenance, reliability, and emissions [13]. AIRBUS's Vahana is an outstanding example of an eVTOL aircraft (Figure 1.2); it was introduced to the public in 2017 and made its first flight in early 2018 [14]. During takeoff and landing, the wings are positioned vertically, causing the propellers' tips to point upwards. Featuring 45 kW motors, the model can attain speeds of up to 220 km/h and travel up to 50 km on a single charge. In 2019 Airbus finalized the cornerstone program that launched the UAM project. Airbus Urban Mobility now has a substantial understanding of the development of its forthcoming UAV attributable to the crucial insights gleaned from Vahana.



(a) Vahana; takeoff phase



(b) Vahana; cruising phase

**Figure 1.2** AIRBUS eVTOL aircraft Vahana [14]

## 1.2 Literature Review

### 1.2.1 Aerodynamic Effects: Stall

Figure 2.1 depicts the lift coefficient over angle of attack for an airfoil [15]. At small to moderate AOA,  $C_L$  changes linearly with  $\alpha$ . In this region, the flow does not separate from the airfoil surface, as seen by the streamline image on the left side of Figure 1.3. As  $\alpha$  increases, however, the flow tends to detach from the top airfoil surface, producing a wide wake of comparatively "dead air", as seen on the right side of Figure 1.3. Within this divided zone, the flow is reversed, and a portion of the flow is traveling in the opposite direction to the

freestream. This divided flow is a result of viscous forces. The separated flow at high AOA causes a dramatic fall in lift and a significant rise in drag; under these conditions, the airfoil is stalled.

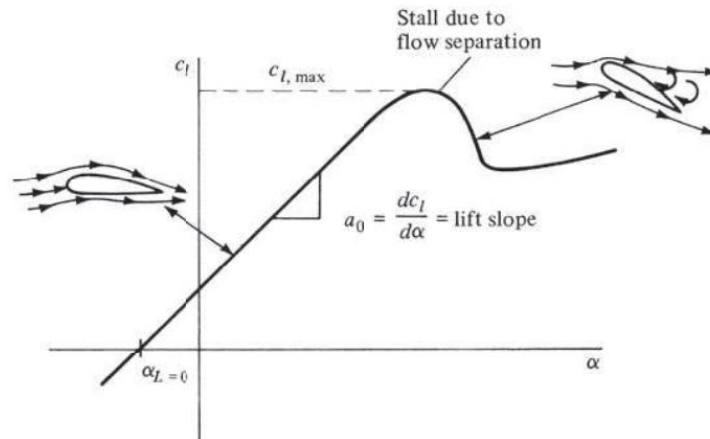


**Figure 1.3** Variation in lift-coefficient with angle of attack for an airfoil [15]

### 1.2.2 Aerodynamic Effects: BLI

Boundary Layer Ingestion is the process of reaccelerating the flow to postpone the flow separation [16]. The propulsion system may be positioned along the span of the wing to reaccelerate the flow. This reduces drag, allowing for a reduction in thrust while keeping the same velocity. Numerous studies described in the following subsections discuss the effects of BLI.

### 1.2.3 Propeller/Wing Interaction

#### *Tractor propeller*

Tractor configuration in aviation refers to an airplane designed in the usual form with the engine situated in front of the propeller (Figure 1.4). Hence, the plane travels through the air by being pulled. The flow field above the wing is affected by the propellers' flow field when propulsion is placed upstream of the wing. Local wing flow is affected by the combined effects of both axial and tangential velocity components of the propeller, which influences the lift distribution and wing stresses [17]. Research has shown that, especially when the propellers are driven extensively, the lift distribution of a wing with propellers deviates greatly from the optimum lift distribution of a wing without propellers [21, 22].

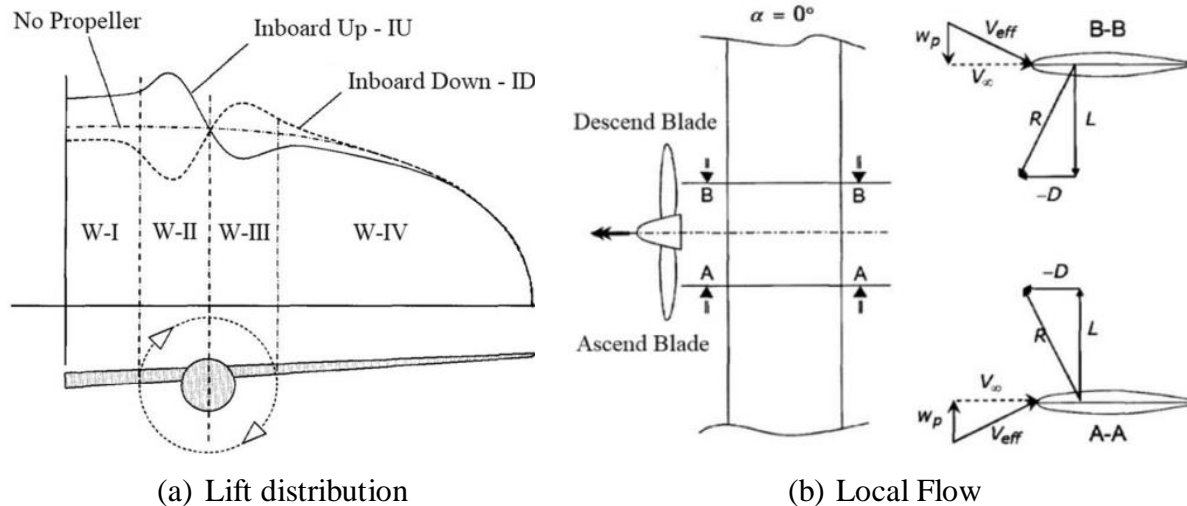


**Figure 1.4** The wing's exposure to propeller flow [17]

Figure 1.4 depicts the exposure of wing to the propeller flow [17]. The lift in the W-II region is increased because of two reasons. Firstly, the upwash induced flow generates a higher local angle of attack, and secondly, the dynamic pressure of the flow is raised. This occurs because the propeller blade rotates with its rising end close to the wing root, which is in the inboard up direction. This creates a distortion in the vorticity field that affects the lift distribution not only in the region just behind the propeller disk but also in the W-I and W-IV regions. Therefore, the effect on lift is not limited to a specific area. Such shifts in lift distribution are frequently viewed as a destabilizing factor in tractor designs. The vertical location of the propeller in respect to the wing is crucial since it modifies the axial velocity and thus the wing surface area impacted by the propulsion flux. The longitudinal location of the propeller in respect to the wing has minimal effect on the lift distribution of the wing.

### *Pusher propeller*

In a pusher layout, the propeller is situated behind the corresponding engine [18]. The propeller's thrust pushes toward the engine rather than away from it in a pusher configuration (Figure 1.5). However, simply turning the engine and propeller around is not enough to transform an aircraft from a tractor to a pusher configuration since the propeller would still be "pulling" the aircraft backward. Assuming that the engine cannot be driven in reverse, the propeller's "handedness" must be altered. Some contemporary engines built for light aircraft include a thrust race that can be used for both "push" and "pull," whereas others require a distinct component depending on which mode they are working in [19].



**Figure 1.5** Piaggio P.180 Avanti; pusher configuration aircraft [20]

It is possible for a pusher to have a shorter fuselage, cutting down on both the wetted area and the overall mass of the aircraft [21]. When compared to the tractor arrangement, the stabilizing effects of a pusher propeller near the tail of the fuselage are clear. A pusher requires less vertical tail area for stabilization and hence exhibits less weathercock effect [22]; during the takeoff roll, it is often less vulnerable to crosswind [23]. Placing the blades behind the wing improves efficiency by reaccelerating the flow and delaying the stall, resulting in less drag. However, it is generally a slight benefit in comparison to the airframe's negative impact on propeller efficiency [24].

### *Summary*

Despite the front-mounted propeller's tendency to cause instability and the revolving slipstream's detrimental effects on control, most tractors have acceptable in-air handling characteristics. It is evident that the pusher's ability to take off and land is greatly hampered by its inability to spin its wings adequately due to its limited rear ground clearance, even with a smaller propeller. Configuration changes to provide enough ground clearance led to decreased in-flight performance. Aircraft featuring distributed wing-mounted propellers suffer less in this aspect, although they share most the pusher's other performance-degrading factors.

### 1.2.3 DEP: Numerical Studies

The use of virtual actuator disk models in studying the interaction between propulsion and wings is common due to their accuracy, efficiency, and simplicity. In these models, blade element theory is employed to calculate the forces acting on each radial segment of the propeller. By examining the lift and drag coefficients at different points along the radius of the disk, the resulting thrust and torque can be determined. The increase in pressure within the



actuator disk is directly proportional to the amount of thrust generated by the propeller per unit of disk area. Equation 1.1 expresses this relationship.

$$\Delta p = \frac{NdT}{2\pi r dr} \quad (1.1)$$

where the thrust across the whole actuator disk is represented by  $dT$  and  $N$  represents the number of blades.

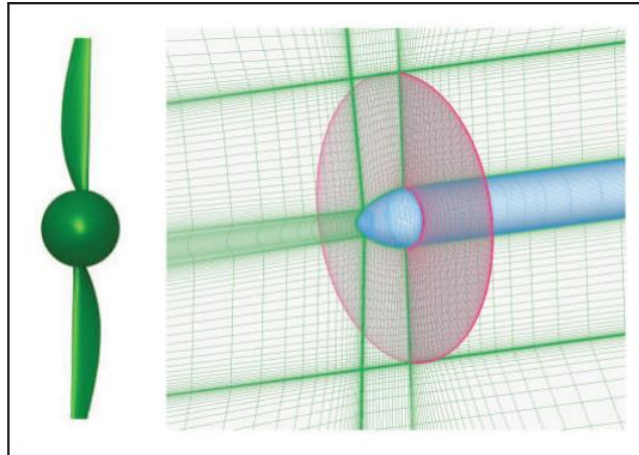


**Figure 1.6** Propeller and Actuator disk [25]

This subsection contains results from numerical simulations (CFD) on the impact of distributed propulsion on wing aerodynamics. Most of the research examine the effects of different wing designs on aerodynamics. Configurations may vary in geometry, number, and position of propellers. Using DEP to reduce the wing size while retaining lift is considered in a few articles. These configurations are also compared to wings of standard size. The angle of Attack and the angle of deflection of the propellers are frequently regarded independent variables, whereas lift and drag are dependent variables and the primary focus of attention.

In one study, the actuator disk model, CFD approach, and momentum theory were used to analyze the propeller-wing system [26]. Using the velocity of the stream behind the blades, which is based on the momentum theory, is proposed as a method for determining the lift coefficient of the layout. OpenVSP evaluated the effect of different number of blades on the lift coefficient distribution using the actuator disk model. Calculations and simulation were performed using a commercial code based on the CFD approach, and the  $k-\omega$  SST model was utilized to investigate the interaction of the propeller-wing system. The authors conclude that the effect of a pull-type propeller's stream on a wing is equivalent to that of an incoming flow that has the same speed and AOA. The rise in speed will increase the wing's lift. Figure 1.7 depicts lift distribution along the span with 2 and 4 propellers. For the future study, the authors

suggest that the CFD slipstream analysis approach should be further tested. Moreover, the influence of distance between propulsors and wing's leading edge must be studied in detail.

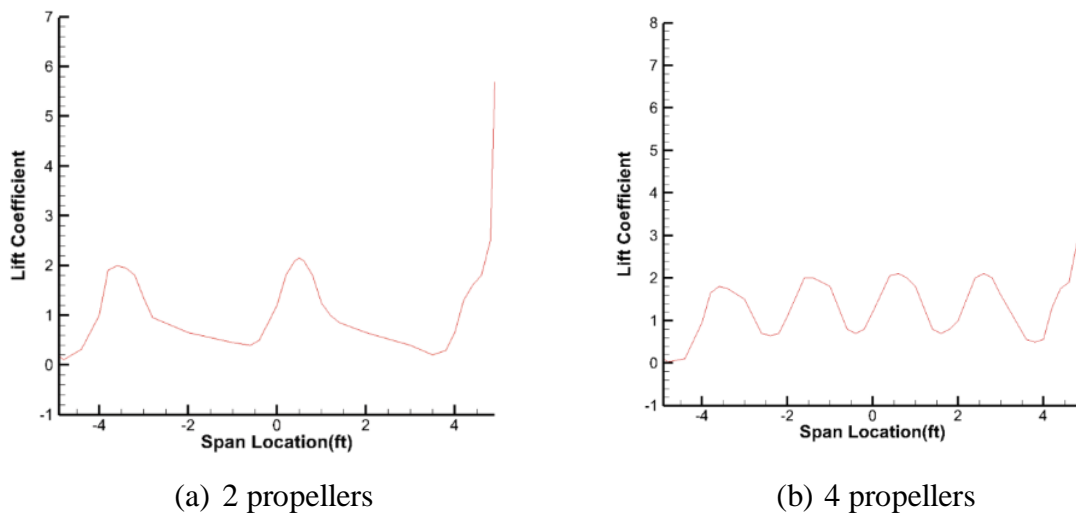


**Figure 1.7** Lift distribution along the span [26]

Another study investigated the effect of shifting the location of the propellers on the aerodynamic performance characteristics of a distributed electric propulsion system with BLI in a wing [27]. The ratio of lift to drag is seen in Figure 1.8. The authors implemented thirteen propellers with a blade radius of 40 mm. Maximum lift-to-drag ratio is around 12.5 when the propelling components are positioned 31.5% above the trailing edge. When the propellers were lowered in relation to the trailing edge, more thrust was noted. However, the wing's aerodynamic performance was worse.

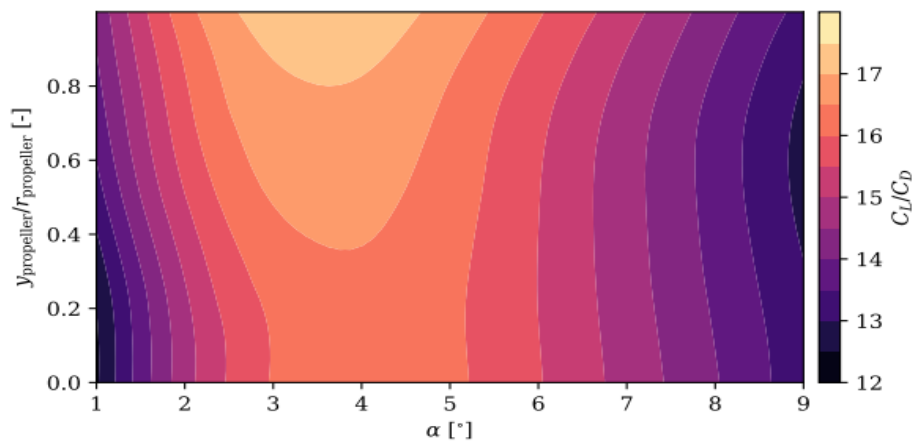


**Figure 1.8** Lift-to-drag ratio at different angles of attack and propeller positions [27]

According to the authors' recommendation, the influence of horizontal distance between wing's trailing edge and propeller should be investigated in the same manner as positioning the propellers too close to the trailing edge may result in vibrations. Computational fluid dynamics

(CFD) and Kriging surrogate models were used to examine the influence of DP [28]. The results reveal that across a wide range of design space, the effect of BLI positively influences the aerodynamics and efficiency at a small AOA, whereas an unsuitable arrangement would have detrimental effects on efficiency.

#### 1.2.4 DEP: Experimental studies

Using a sequence of wind tunnel experiments, one research compared and examined the aero-propulsive coupling parameters at varying freestream velocity, propeller RPM, and deflection angles [29]. Under the experimental parameters of 15–25 m/s freestream flow and 4–16 degrees of attack, the authors compared different lift-augmentation settings to the baseline setup without a propulsion unit.  $C_L$  is shown against an AOA as a function of throttle in Figure 1.9. In comparison to the clean arrangement,  $C_L$  decreased between 0% and 20% for the throttle at every experiment airspeed. Once the power unit installed on the top wing surface of the DEP aircraft was operating at a windmill situation, lift was reduced because the flow just above power source parted from the wing surface.

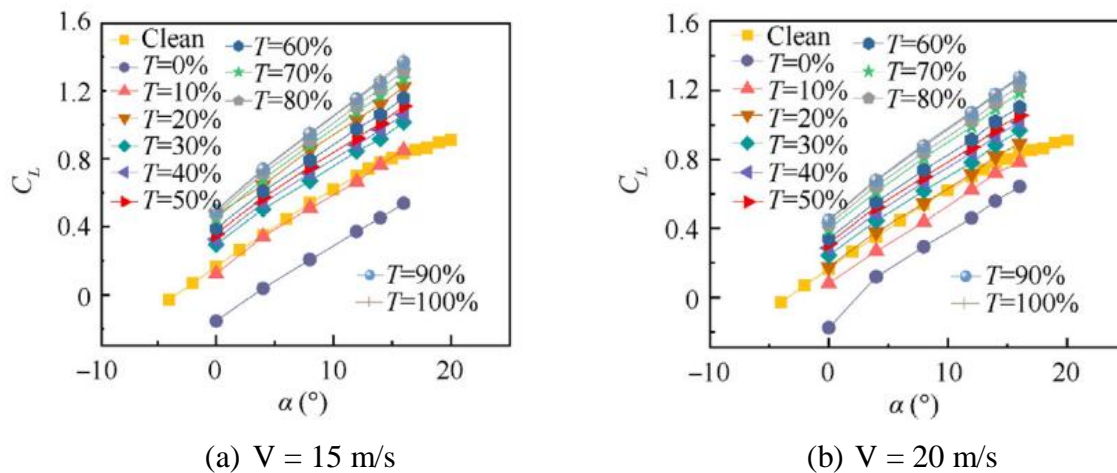


**Figure 1.9** Lift coefficient at 15 and 20 m/s [29]

The study confirmed the efficiency of the BLI's in DEP configurations. As a result of the DEP's intervention, the lift-to-drag ratio at cruising  $AOA = 4^\circ$  may be enhanced from 7.2 to 21.57 and the maximum  $C_L$  at  $AOA = 4^\circ$  can be augmented from 0.836 to 1.429. Regarding the deflectable surface of the thruster, it may also considerably enhance aerodynamic efficiency. With a  $\delta_T$  value of  $30^\circ$ , the maximum  $C_L$  may be elevated to 2.28, which is 1.6 times more than cruising layout. The surface deflection eliminated the increase in drag brought on by the propulsion unit at a small AOA, specifically when the throttle was less than 20%. According to the authors' recommendations, utilizing such a phenomenon to enhance DEP aircraft design and optimization requires more research.

Another experimental study discovered that the addition of a DP system may enhance lift 2.6 times at  $0^\circ$  AOA and improve the wing's stall angle (Figure 1.10) [30]. When positioned above and beyond the wing, the DP system provides the most efficiency of the three evaluated designs. Higher throttle levels are substantial when used to boost lift at  $0^\circ$  angle of attack but have a little effect on lift increment when used to postpone stall.

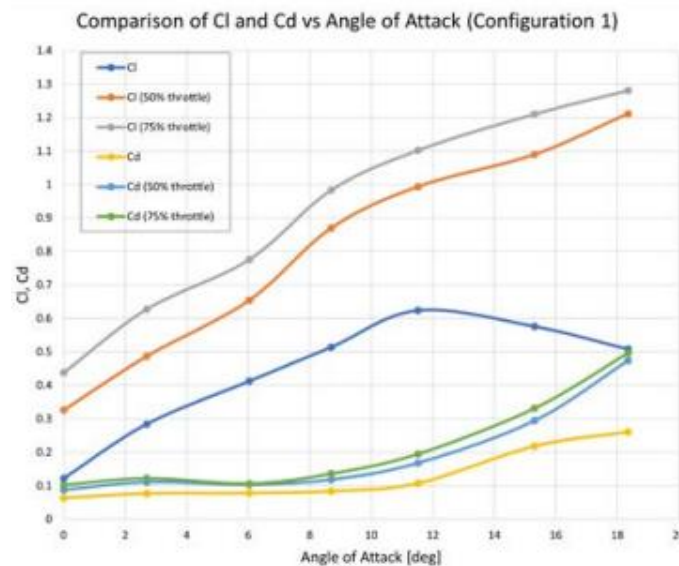


**Figure 1.10** Lift and Drag vs AOA at different throttle [30]

Future research can focus on reducing this impact to achieve more accurate lift and drag characteristics, as stressed by the authors. Attaching propellers to the wing to eliminate relative motion or reducing the errors caused by relative motion are potential options.

The third article in this list covered an experimental study of the aerodynamic interaction between DP [31]. This study attempted to evaluate the influence of distributed propellers on one another, as opposed to prior research which focused exclusively on interactions between the wing and propeller. At the thrust level that corresponds to maximum efficiency and with a tip distance equal to 4% of the blade radius, the contact resulted in a loss of 1.5% in propellant efficiency. This efficiency penalty is greater at lower thrust levels and is independent of propeller rotation direction for a constant blade-pitch angle. It is especially noticeable at angles of attack apart from zero, in which case the contact results in an increase in propeller normal force. Although this study's findings explain certain interaction processes, other questions remain unresolved. Specifically, it is crucial to investigate how the localized unstable load on the propellers is influenced by the instability of aerodynamic interactions between neighboring propeller tips and tip vortices.

Another study investigated the technique for achieving high lift by putting blades directly ahead of the wing and exploiting interaction forces. [32]. The results indicate that, for constant rotor power, there exists an ideal propeller size that optimizes the growth in lift. It was also discovered that for the low thrust, the relationship between lift and DEPS angle of inclination is quite weak.

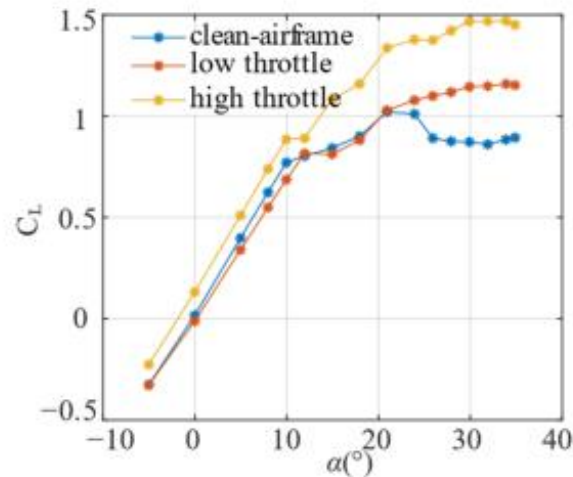


**Figure 1.11**  $C_l$  vs AOA [33]

Another research implemented both CFD analysis and experimental investigation to determine the influence of DP on an aircraft's flying characteristics [33]. Specifically, the angle of attack at stall was studied by conducting an airplane tunnel experiment. According to the data, the angle of stall for an aircraft without DP was around 21 degrees, whereas the angle of stall for an aircraft with DEP was 30 degrees (Figure 1.11). Using the DP system improved the angle of stall significantly, as seen by the findings.

### 1.3 Summary of the Literature & Research Gaps

The literature review on distributed propulsion and its impact on wing aerodynamics has highlighted several research gaps that need to be addressed to gain a more comprehensive understanding of this phenomenon. One such gap is the influence of the horizontal distance between the wing's trailing edge and the propeller on aerodynamics. While some studies have investigated the effects of varying the distance between the wing and propulsors, the focus has been primarily on the vertical distance. There is a need for further research to determine how changing the horizontal distance could affect the flow of air around the wing and propeller and how this, in turn, could affect aerodynamic performance. Another research gap is the optimization of DEP aircraft design using the phenomenon of deflection to enhance aerodynamic efficiency. Deflection refers to the ability of the deflectable surface of the thruster

to direct airflow and generate additional lift. While some studies have examined the use of deflection in DEP aircraft design, further research is needed to determine how best to optimize this phenomenon for maximum aerodynamic efficiency. In addition to these gaps, the review has also suggested the need for more research on the effects of propeller stream on wing lift and the influence of the distance between propulsors and wing's leading and trailing edge. Specifically, the use of CFD slipstream analysis and wind tunnel experiments could provide valuable insights into these effects and help to refine current design principles for DEP aircraft. Overall, the literature review has highlighted several areas where further research is needed to gain a more comprehensive understanding of distributed propulsion and its impact on wing aerodynamics. Addressing these research gaps could help to unlock new opportunities for more efficient and sustainable aircraft design in the future.

## 1.4 Research Aim and Objectives

The aim of this research is to experimentally investigate the effectiveness of distributed electric propulsion on wing aerodynamics and stability. Specifically, the objectives of the research are to:

1. Assess the influence of the distance between trailing edge and propulsion elements on the net forces acting on of the wing.
2. Assess the indirect influence of the propellers on lift and drag forces in order to gain more comprehensive understanding of how are affected by the flow acceleration around the wing.
3. Identify the optimal throttle settings for the propellers and freestream velocity to achieve steady level flight.

# Chapter 2 – Experimental Setup

---

*The objective of research methodology is to describe the reasoning behind research strategy; in this chapter, the chosen collecting techniques, analysis methods and other important aspects of the work are described and justified.*

## 2.1 Introduction

The research utilizes wind tunnel to experimentally investigate the aerodynamics of the wing, specifically examining the effectiveness of distributed electric propulsion on wing aerodynamics. The methodology includes a detailed design description of the experimental setup, including the characteristics of the independent and dependent variables, and the measuring process. Two separate experiments are conducted to answer the research questions posed in the preceding chapter, with one experiment focusing on assessing the influence of the distance between trailing edge and propulsion elements on wing aerodynamics, and the other experiment identifying the optimal throttle level for the propellers and freestream velocity to achieve steady level flight. The results of the experiments are analyzed and presented, providing empirical evidence on the effectiveness of distributed electric propulsion on wing aerodynamics, with implications for future aircraft design and the advancement of electric aviation technology.

## 2.2 Design description

### 2.2.1 Baseline wing

The ability to create lift with much less drag makes airfoils one of the most effective lifting forms. Aerospace engineering uses airfoils in the design of airplanes, propellers, rotor blades, and wind turbines, among other applications. NACA 2418 airfoil was chosen to model the baseline wing for this research (Figure 2.1). The wing was designed with CAD and manufactured using a 3D printer. The dimensions of the wing are provided in Table 2.1. Since the primary objective of this study was to assess the efficacy of DEP, the choice of airfoil was not as important. Therefore, the primary requirement for airfoil selection was sufficient thickness to fit the 12-mm-diameter steel rod as a support in the wind tunnel. The working space in the wind tunnel is 600 millimeters wide, thus a span of 576 millimeters has been chosen for the wing to ensure a clearance between the tunnel walls and the wingtips. Moreover, in the following experiments, the excess space was occupied by additional supports for the propulsion elements.

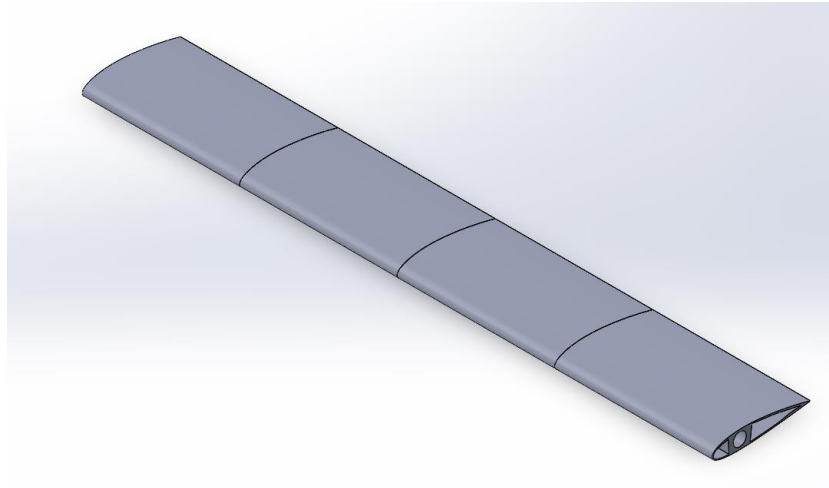


**Figure 2.1** Baseline Wing

Table 2.1 Wing dimension

Span	Chord	Aspect Ratio
576 mm	90 mm	6.4

### 2.2.2 Propeller characteristics

The propellers utilized in this study are forward and reverse rotation propellers. Used in conjunction with a high-speed brushless motor and RPM controller of 12A or above. For a comprehensive study of the aero-coupling effect of DP propeller with 128 mm diameter was used (Figure 2.2).



**Figure 2.2** 5040 Propeller

### 2.2.3 Brushless Motor

The distributed propulsion system consists of two pusher propellers with motors mounted on the rod supported by plywood sheets. Brushless motors are a type of permanent magnet synchronous motor, which are fed from a DC circuit via an inverter controlled by a feedback controller [34]. The controller supplies the motor phases with the voltages and currents necessary to produce the required torque and run at the desired speed. This controller replaces the brush-collector assembly used in DC collector motors. The brushless motors can operate with winding voltages in a pure sine wave form or in a piecewise step form (e.g., in



block commutation). This research utilized a highly efficient 2205 motor with 1700KV and a suggested ESC of 40-60A (Figure 2.3).



**Figure 2.3** Brushless Motor

#### 2.2.4 Wind Tunnel

A wind tunnel is utilized to imitate the movement of an object by forcing airflow. This research makes use of a subsonic Tecquipment AF1600S wind tunnel. The wind tunnel provides precise data appropriate for research. TecQuipment provides an extensive selection of instruments, which includes a computerized data collecting system. Air enters the AF1600 through a grille and a honeycomb flow straightener (Figure 2.4).

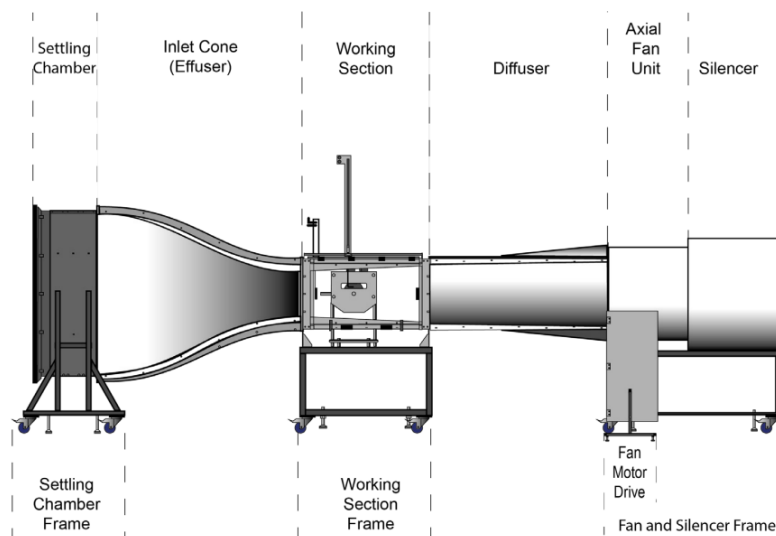


**Figure 2.4** Wind tunnel schematics

It then enters an aerodynamically built effuser (a cone) that linearly accelerates the air before it enters the operating area. The air then flows through a diffuser before entering an axial fan at variable speed. The grille serves as protection for the fan against harm caused by loose items. The air exits the fan, travels through a silencer device, and finally returns to the environment. An electronic drive system in a separate on/Off unit attached to the tunnel's instrument frame with other ancillary components controls the speed of the axial fan (and, as a

result, the airspeed in the test section). The testing section is square with curved edges and an acrylic wall at the top and bottom. The dimension of the working section is 600x600x1200 mm. The sides consist of full-length acrylic panels, one of which is hinged at the top and the other of which is detachable. The entire structure is supported by an aluminum frame. Each side panel is equipped with a holder for wind tunnel models. Two Pitot devices are mounted on top of the working part to monitor the static pressure. The experiments were conducted under the conditions listed in Table 2.2.

Table 2.2 Operating conditions

Ambient Temperature, C°	18°
Relative Humidity	30%
Air density, kg/m <sup>3</sup>	1.211

### 2.2.5 DEP Configuration

The experimental layout is comprised of a NACA2418 wing and a DEP with two symmetrically positioned propellers along the span. The propellers with motors are attached to the wing via the mounts and 5 mm rod supported by the side and center supports of the wing. The supports are 5 mm thick, therefore the total span of the wing is 591 mm.

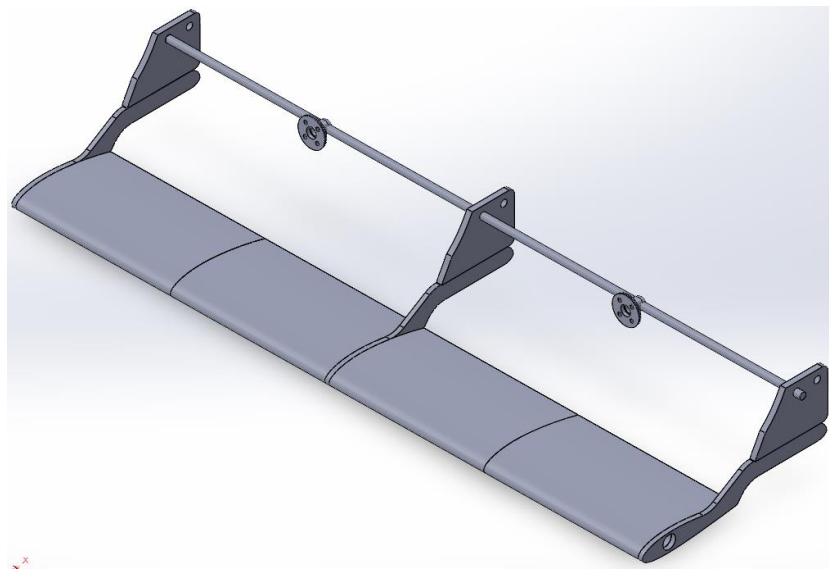


Figure 2.5 CAD model of DEP

## 2.3 Measurement process description

### 2.3.1 Angle of Attack

The angle of attack is an independent variable that is controlled by the Balance Angle Feedback device (Figure 2.6). The angle of attack of the model is subsequently transmitted to

(VDAS®). Along with the other experimental data obtained, the model's angle is recorded on a suitable computer.

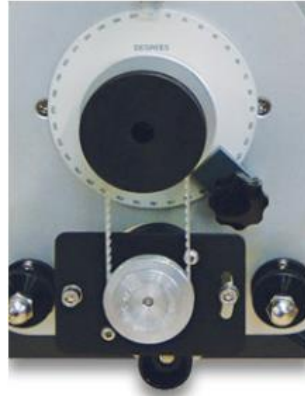


**Figure 2.6** Balance Angle Feedback

### 2.3.2 Freestream Velocity & Pressure

The Pitot-static tubes and other pressure-sensing equipment attached to the wind tunnel are pressure-sensing devices, and the Dual Differential Pressure Unit monitors and displays these pressures in comparison to the atmosphere or differential pressures (Figure 2.7). A Pitot-static tube is fixed to the fore-aft traverse or upstream of the test model in the working part of the wind tunnel. This enables one to navigate a model's "wake." The changeable vertical position of the tube is shown on a digital indicator. Any location can be used to reset the digital indication to zero.



(a) Pitot tube



(b) Dual Differential Pressure Unit

**Figure 2.7** Pressure measuring device

Since the flow is incompressible ( $V_\infty < 100\text{m/s}$ ), pressure difference can be found from:

$$\Delta p = \frac{\rho V_\infty^2}{2} \quad (2.1)$$

where  $\rho$  is air density:

$$\rho = \frac{P_\infty}{RT_\infty} = 1.211 \frac{\text{kg}}{\text{m}^3} \quad (2.2)$$

### 2.3.3 Lift and Drag

The Three-Component Balance is a device used to measure aerodynamic forces. It is designed to work with TecQuipment's Subsonic Wind Tunnel (AF1600) and can measure forces in three dimensions. The device is restricted to move only in the plane parallel to the mounting plate, but it can freely spin about the horizontal axis, providing the necessary three degrees of freedom. The loads imposed on the model being tested are transmitted through cables to three load cells equipped with strain gauges. These load cells are connected to an amplifier and a display module that is controlled by a microcontroller.



**Figure 2.8** Three-Component Balance

### 2.3.4 Propeller RPM

To set the throttle of the motor, the Arduino due board is utilized. Arduino due is the first board of the Arduino family based on the Atmel SAM3X8E 32-bit microcontroller with an ARM processor based on the ARM Cortex-M3 core. With a clock frequency of 84 MHz and a 32-bit architecture, it can perform most integer operations of 4 bytes in a single clock cycle. Testing the speed of a brushless motor involves applying PWM to the motor and varying the duty cycle from minimum to maximum. The PWM application implies the measurement of RPM of the motor and tracked in an effort to determine the variation of RPM with respect to the PWM width changes. The Arduino code that was used is provided in appendix A.

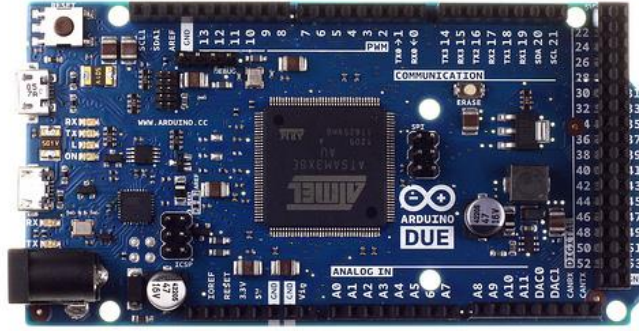


**Figure 2.9** Arduino board

## 2.4 Experiment procedure

### 2.4.1 Experiment #1: Effect on Net Forces

The objective of this experiment is to investigate the effect of propeller placement on the performance of a wing with two propellers placed behind it. The study will focus on four different configurations that vary in the placement of the propellers relative to the trailing edge of the wing. The study will measure the net horizontal and vertical forces acting on the wing and compare the results between the four configurations. The experiment will be conducted in a wind tunnel with a constant freestream velocity of 15 m/s. The wing model will be fixed in the wind tunnel and the four propeller configurations will be tested sequentially. The propellers will be powered by an electric motor and the throttle of the propellers will be maintained at 20% and 40% throughout the experiment. The experiment will involve measuring the net horizontal and vertical forces acting on the wing model for each of the four configurations. The four different configurations that differ in both horizontal and vertical displacement are outlined in Table 2.3.

Table 2.3 Configurations

Configurations	Horizontal Displacement	Vertical Displacement	Propeller Diameter
Configuration 1	0.11C	0.21C	128 mm
Configuration 2	0.33C	0.21C	128 mm
Configuration 3	0.33C	0.71C	128 mm
Configuration 4	0.11C	0.71C	128 mm

To determine the impact of propeller placement on wing performance, a force balance system will be attached to the wing model to measure the net vertical and horizontal forces acting on the wing. The force balance system will consist of three components, two perpendicular to the wing and one parallel to the wing. To ensure reliable results, each configuration will be tested a minimum of four times. The recorded data will be analyzed to

compare the results. The net vertical forces acting on the wing for each configuration will be compared to identify the configuration that produces the highest net force. From a set of four measurements, we can calculate both the average value and the standard deviation. The standard deviation is a measure of the amount of variation or spread in the data. It indicates, on average, how much each value deviates from the mean. The standard deviation provides information about the spread of the data around the mean, with larger values indicating more variability. By calculating both the average value and standard deviation of a set of measurements, we can gain insight into the central tendency and variability of the data, respectively.

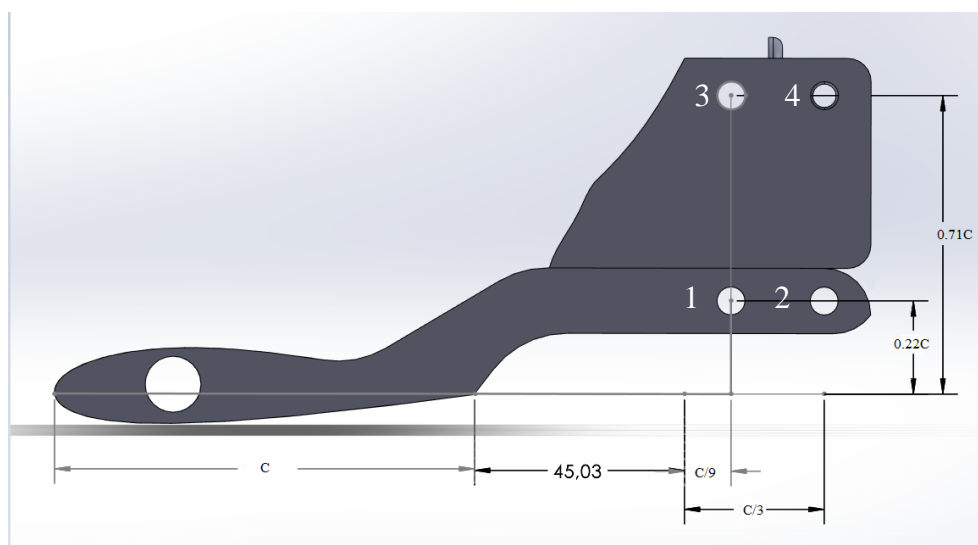
$$\sigma_y = \sqrt{\frac{\sum(F_{yi} - \bar{F}_y)^2}{N}} \quad (2.3)$$

$$F_y = \frac{1}{N} \sum_{i=1}^N F_{yi} \pm \sigma_y \quad (2.4)$$

$$\sigma_x = \sqrt{\frac{\sum(F_{xi} - \bar{F}_x)^2}{N}} \quad (2.5)$$

$$F_x = \frac{1}{N} \sum_{i=1}^N F_{xi} \pm \sigma_x \quad (2.6)$$

In the results section, the values derived from (Eq. 2.4 and Eq. 2.6) will be presented in the form of clear and visually informative plots, facilitating a more comprehensive understanding of the findings.



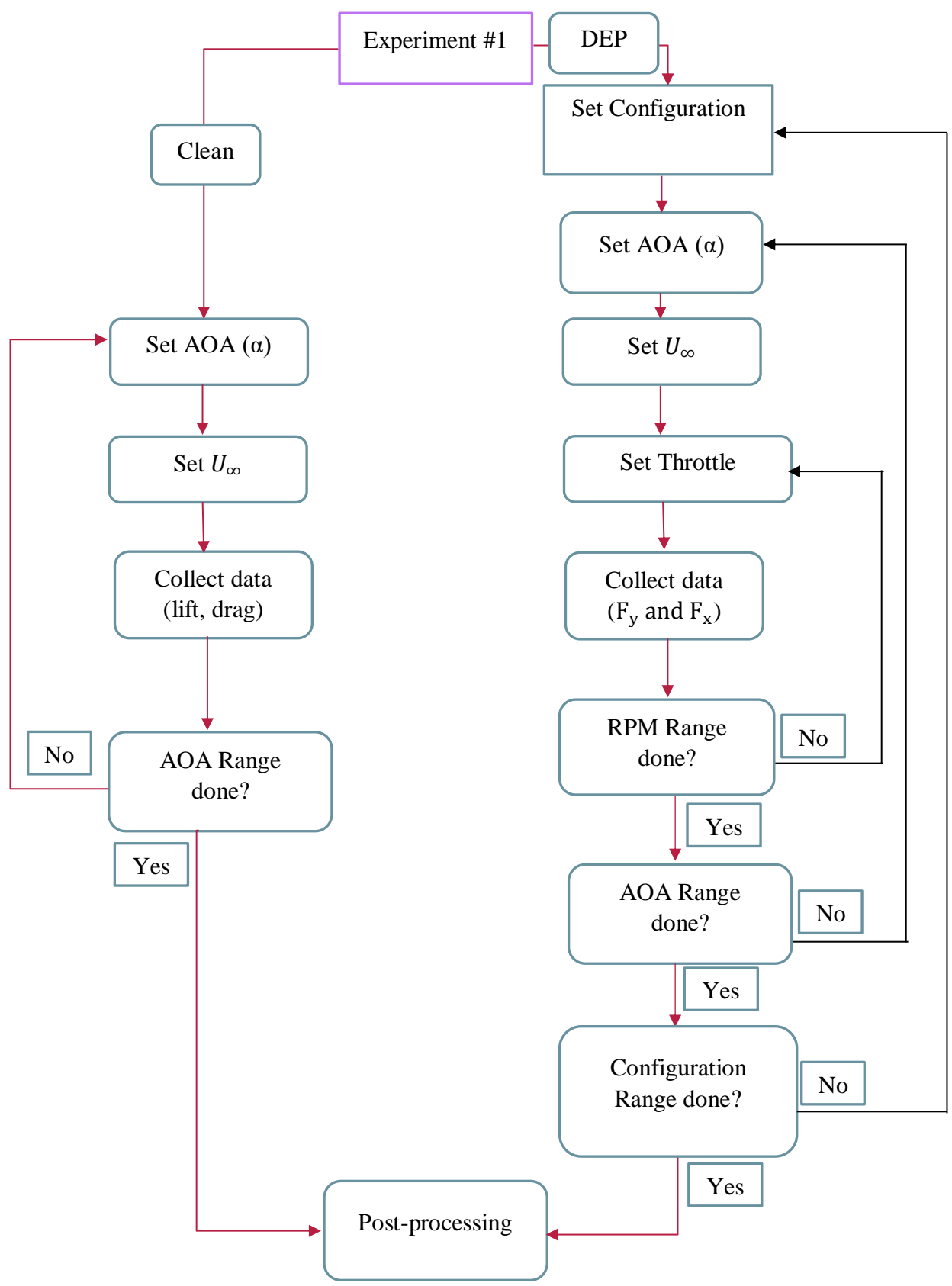
**Figure 2.10** Four configurations

Figure 2.10 depicts the four configurations with the horizontal distance of 0.11C and 0.33C. Note that 45.03 mm is preserved for the motor and mount. The list of independent and dependent variables is given below (Table 2.4). 0.71c was chosen as the vertical distance between rotor and trailing edge to keep the tips of the propellers above the wing. Presumably, this arrangement will increase lift by accelerating the flow on the upper surface of the wing.

Table 2.4 Variables 1

<b>Variable</b>	<b>Type</b>	<b>Range</b>	<b>Step</b>
<b>Angle of Attack (°)</b>	Independent	From -4° to 22°	2°
<b>Throttle</b>	Independent	From 0% to 40%	20%
<b>Freestream Velocity</b>	Constant	15 m/s	NaN
<b>Propeller Deflection Angle</b>	Constant	0°	NaN
<b>Propeller diameter</b>	Constant	128 mm	NaN
<b>Horizontal distance</b>	Varies	0.11C, 0.33C	NaN
<b>Vertical distance</b>	Varies	0.22C, 0.71C	NaN
<b>F<sub>y</sub></b>	Dependent	-	NaN
<b>F<sub>x</sub></b>	Dependent	-	NaN

The following figure represents the progression of the first experiment.



**Figure 2.11** Experiment #1 flowchart

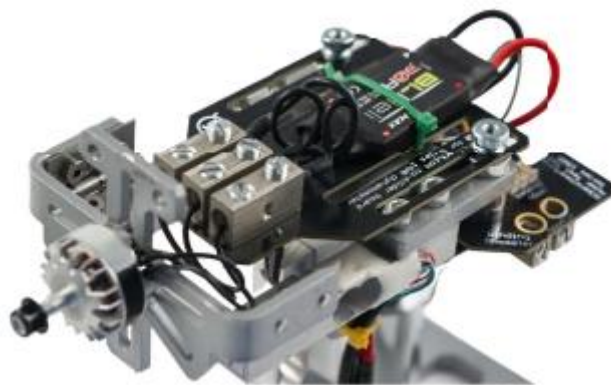


### 3.4.2 Experiment #1: Effect on Lift & Drag

In the second part of the first experiment, the goal is to differentiate between the lift generated by the propellers and the actual lift produced by the wing. The experiment involves measuring the propeller's thrust output at 20% and 40% throttle levels. Subsequently, the resulting values will be subtracted from the previously obtained net horizontal and net vertical forces. By doing so, the propeller's direct contribution to the overall forces acting on the system can be eliminated.

Due to the complex interplay between the wing and propellers, it is essential to measure their performance separately. This is because propellers are particularly sensitive to the presence of the wing, as the disturbed flow and pressure distribution can significantly affect their output. Conversely, the wing is also influenced by the propeller, both directly and indirectly. The direct effect results from the propeller generating thrust that acts on the wing due to their physical connection. The indirect effect arises from the propeller accelerating the airflow around the wing, contributing to its lift. To isolate the direct contribution of the propeller, it is essential to measure its thrust output independently from the wing. This distinction is crucial to analyze the impact of distributed propulsion on the wing's performance, particularly in terms of how it enhances the flow around the wing, resulting in increased speed, higher pressure difference, and greater lift. This information can help optimize distributed propulsion systems for better overall aircraft performance.

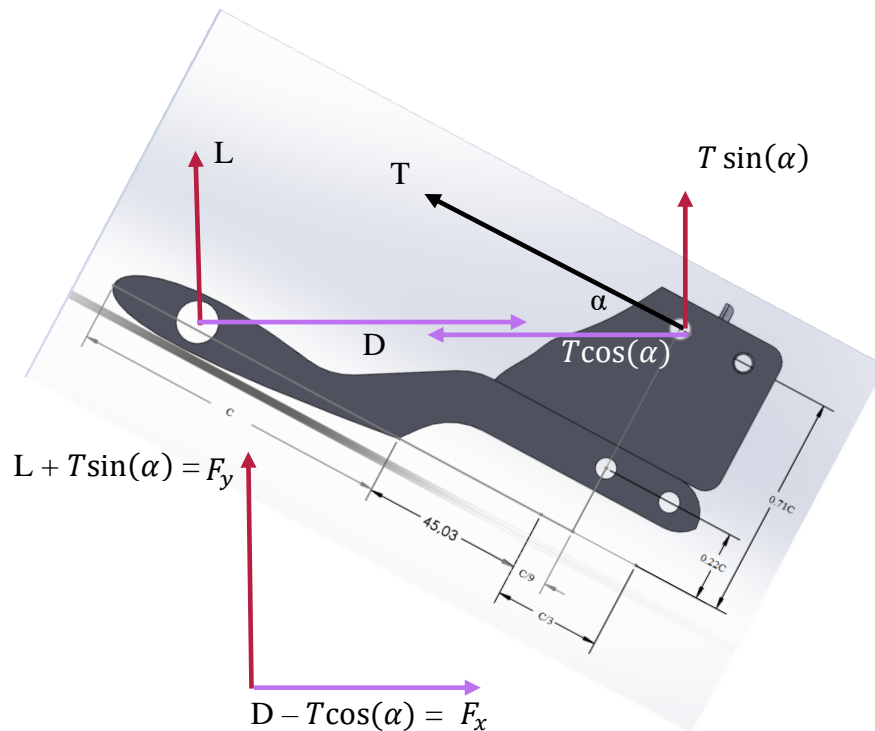
The measurements will be conducted on TYTOROBOTICS 1580 series dynamometer (Figure 2.12).



**Figure 2.12** TYTOROBOTICS 1580

The dynamometer is a device used for measuring the performance of motors, and in this case, it is being used with the RCBenchmark software. This software allows for manual control of the motor through the sending of PWM signals, or the creation of custom automatic testing

scripts using their API. During testing, two different PWM signals, 1200 and 1400, will send to the motor, corresponding to 20% and 40% throttle levels, respectively. Thrust measurements will be then taken and carefully recorded for analysis.



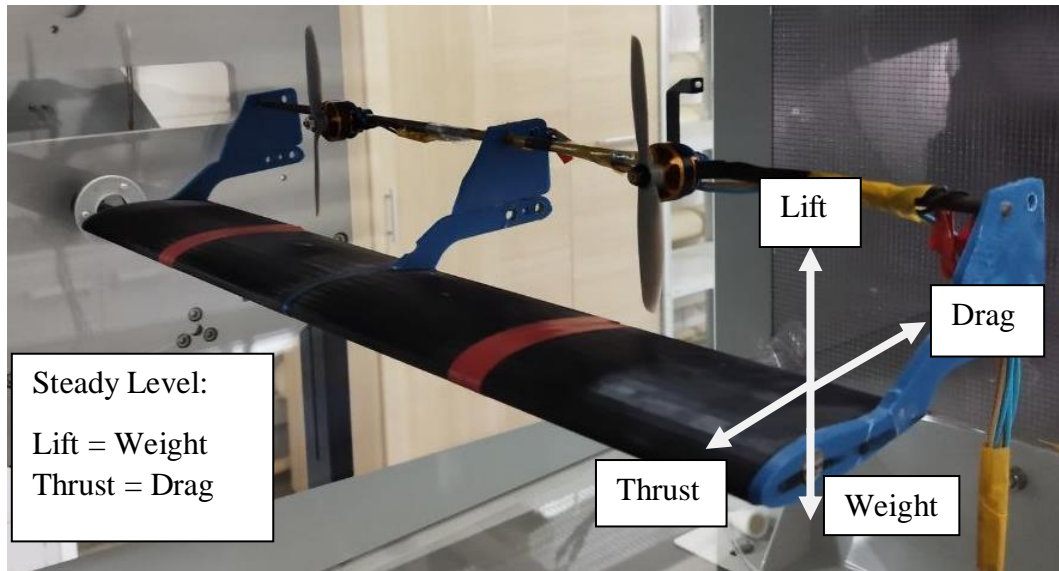
**Figure 2.13** Forces acting on the wing

Figure 2.13 depicts the various forces acting on the wing, including the propulsive lift generated by the propellers. This additional lifting force increases the net vertical force, while the thrust from the propellers acts in opposition to the drag, thereby reducing the net horizontal force. It is important to note that since the propellers are attached to the wing, any drag acting on the entire configuration will be factored into the calculations. As such, the resulting calculations will provide the Lift and Drag forces of the entire DEP configuration, and not just the wing alone. Therefore, the drag forces obtained through measurements and calculations are likely to be noticeably higher than those obtained in a clear wing configuration. However, these results can still offer valuable insights into the aerodynamic impact of propellers on forces, particularly lift.

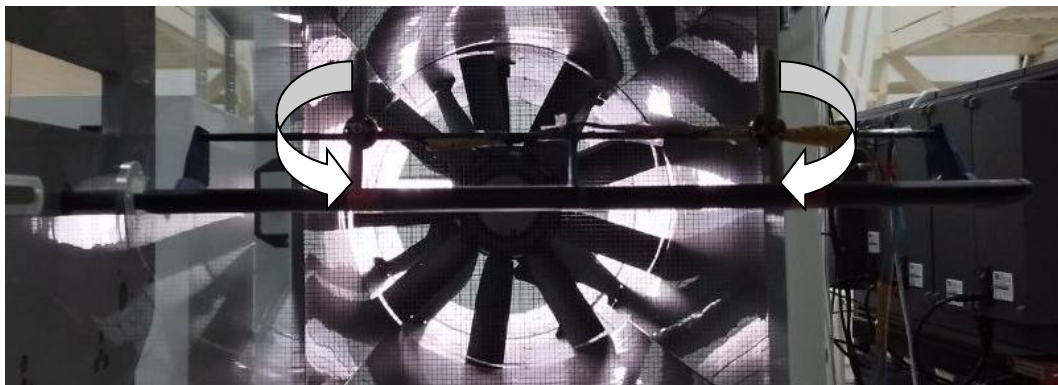
### 3.4.3 Experiment #2: Steady Level Flight

The aim of this experiment is to obtain steady level flight conditions for a wing with 2 propellers. The objective is to adjust the throttle of the propellers as well as the freestream velocity to achieve a zero net horizontal and vertical force on the wing (Figure 2.14). The experimental setup consists of a wind tunnel with a test section that is equipped with the wing

and 2 propellers. The positioning of the propellers corresponds to the fourth configuration from the previous experiment. The wing is mounted in the test section in a way that allows for varying the angle of attack.



(a) isometric view



(b) front view

**Figure 2.14** Fourth Configuration

The throttle of the propellers is controlled using a motor controller, and the freestream velocity is controlled using the wind tunnel fan. The experimental procedure involves the following steps:

1. First, the wind tunnel is turned on, and the freestream velocity is set to a low value. The angle of attack of the wing is set to an initial value, and the throttle of the propellers is set to a low value.

2. The throttle of the propellers is gradually increased while monitoring the net horizontal and vertical force on the wing using force sensors. The freestream velocity is also gradually increased.

3. Once the throttle and freestream velocity have been adjusted to achieve a zero net horizontal and vertical force on the wing, the readings from the force sensors are recorded.

4. The angle of attack is then adjusted, and the procedure is repeated to obtain data for different angles of attack.

5. The data obtained from the experiment is analyzed to determine the optimal throttle and freestream velocity for achieving a zero net horizontal and vertical force on the wing. Overall, this experiment will provide valuable insights into the aerodynamic performance of the wing with 2 propellers, and the data obtained can be used to optimize the design and performance of similar aircraft.

Table 2.5 Variables 2

<b>Variable</b>	<b>Type</b>	<b>Range</b>	<b>Step</b>
<b>AOA (°)</b>	Independent	From 2° to 20°	2°
<b>F<sub>y</sub></b>	Constant	5 N	NaN
<b>F<sub>x</sub></b>	Constant	0 N	NaN
<b>Propeller diameter</b>	Constant	128 mm	NaN
<b>Configuration</b>	Constant	4th	NaN
<b>Freestream Velocity</b>	Dependent	-	NaN
<b>Throttle</b>	Dependent	-	NaN

The following picture depicts the progression of the second experiment.

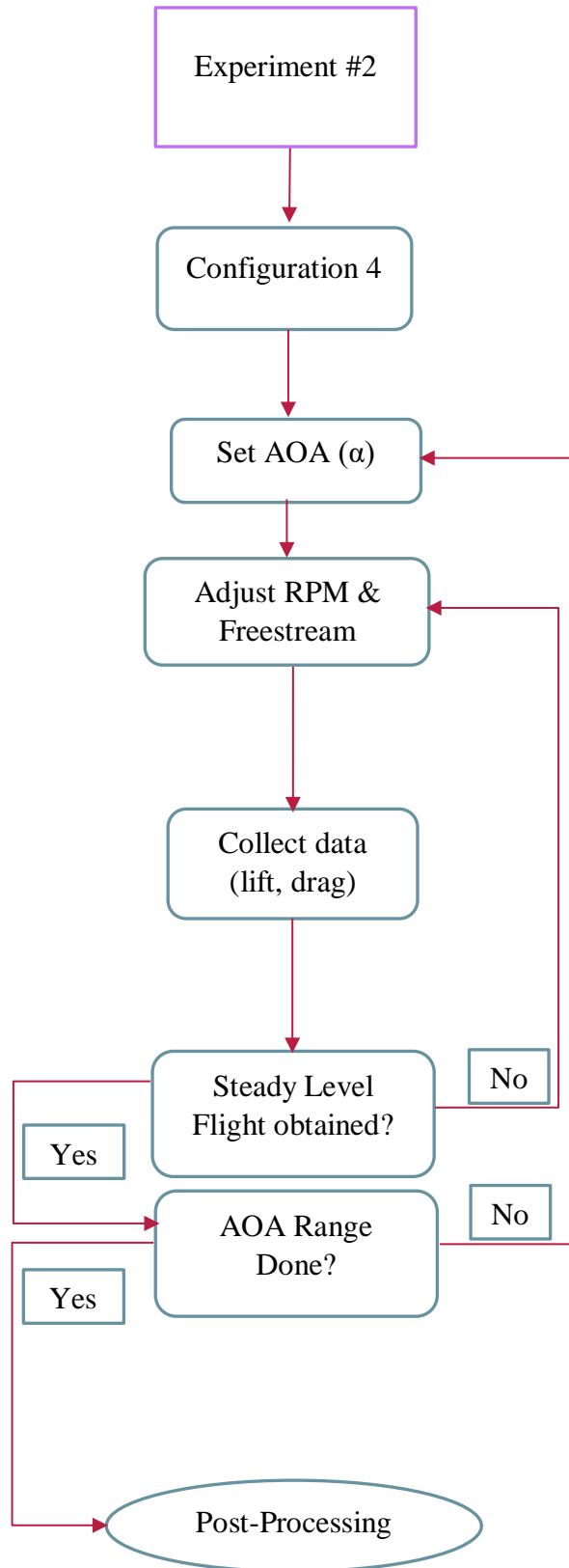


**Figure 2.15** Experiment #2 flowchart

# Chapter 3 – Results & Discussion

---

*This chapter presents the findings of the experimental work. This chapter also discusses the results of both experiments and highlights the key observations*

## 4.1 Experiment 1: Propeller Position Effect on Net Forces

The experiment aimed to investigate the effect of propeller placement on the performance of a wing with two propellers placed behind it. Four different configurations were tested, varying in the placement of the propellers relative to the trailing edge of the wing. The net horizontal and vertical forces acting on the wing were measured for each configuration, with the throttle of the propellers maintained at 20% and 40% throughout the experiment. The results obtained from the experiment were analyzed to determine the effect of propeller placement on the performance of the wing and to identify the configuration that produces the highest net vertical force and lowest net horizontal force. To ensure the credibility of the results, the experiment for the single angle of attack (AOA) was conducted at least 4 times. The mean value of the net vertical force was taken, and error bars were plotted in MATLAB, showing the  $\pm$  deviation of the values.

### 4.1.1 Net Vertical Force

The measured data, expressed in terms of net vertical force, indicated that the performance of each configuration varied considerably. Upon initial observation, it was indicated that the stall occurred at a 10 degrees angle of attack. However, upon further analysis, it was found that after reaching 12 degrees AOA, the net vertical force continued to increase. This unexpected behavior of the net vertical force could be explained by the fact that the propellers started generating propulsive lift in a more vertical direction. In order to determine with certainty whether it was propulsive lift or an actual stall delay, it is necessary to isolate the direct influence of the propellers on the wing. This can be achieved by measuring the thrust generated by the propellers alone and subtracting the vertical and horizontal components of thrust from the net vertical and net horizontal forces. This step is described in the following subsection.

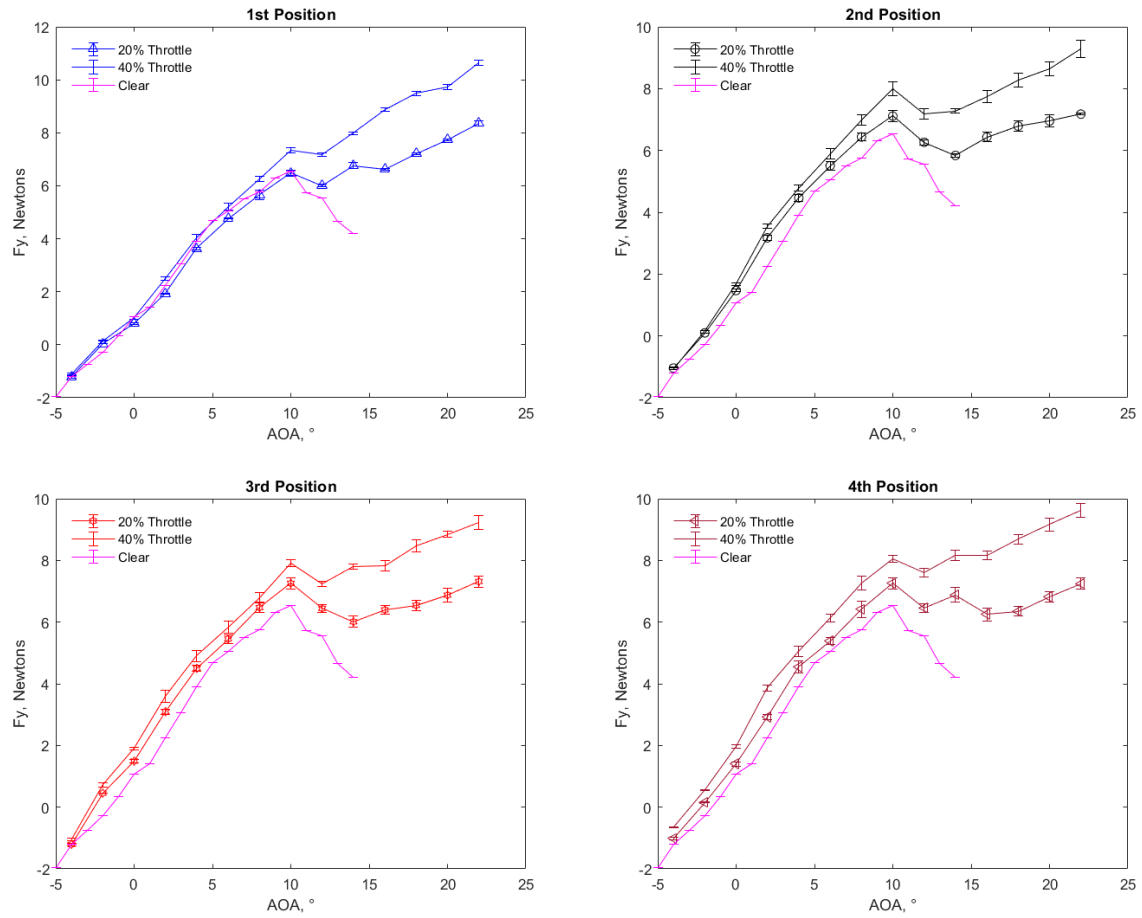
This subsection is focused on the analysis of the net vertical force acting on different propeller configurations, to compare their performances and optimize their position in relation to the flow generated by the wing. The aim of this analysis is to investigate how the various propeller configurations interact with the flow generated by the wing and generate vertical force.

Table 3.1 Net Vertical & Net horizontal forces at  $\alpha = 10^\circ$

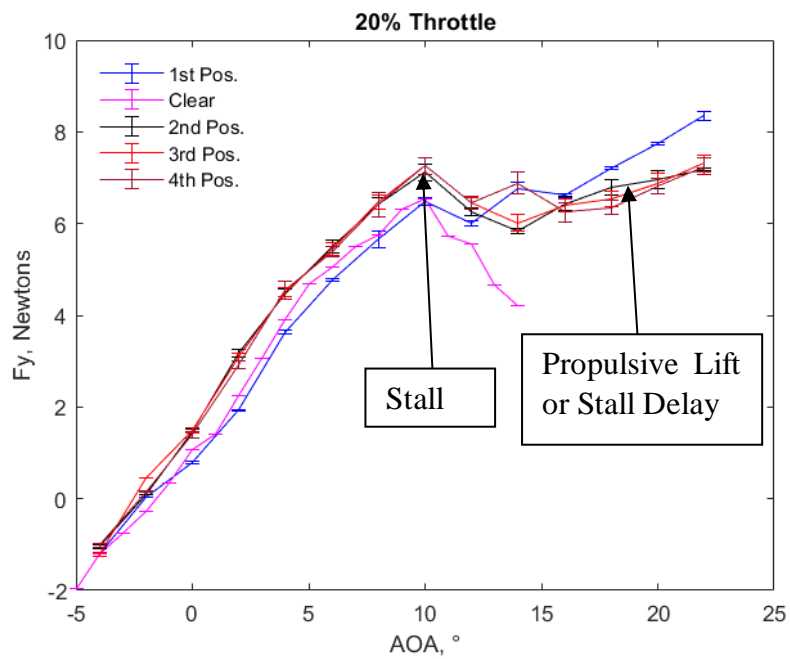
	Clear Wing	Configuration 1		Configuration 2		Configuration 3		Configuration 4	
		20%	40%	20%	40%	20%	40%	20%	40%
Throttle	-	20%	40%	20%	40%	20%	40%	20%	40%
$\bar{F}_y$ , N	6.54	6.48	7.33	7.11	8	<b>7.3</b>	7.9	7.25	<b>8.04</b>
$\bar{F}_x$ , N	0.39	1.34	0.1	<b>1.32</b>	<b>0.01</b>	1.4	0.155	1.67	0.41
Absolute Difference in $\bar{F}_y$ , N	-	-0.06	0.79	0.57	1.46	0.76	1.36	0.71	1.5
Relative Difference in $\bar{F}_y$	-	-0.91%	12%	9%	22%	<b>12%</b>	21%	11%	<b>23%</b>
Absolute Difference in $\bar{F}_x$ , N	-	0.95	-0.29	0.93	0.38	1.01	-0.235	1.28	0.02
Relative Difference in $\bar{F}_x$ , N	-	243.5%	74%	<b>238%</b>	<b>97%</b>	266%	60%	328%	5.1%

Table 3.1 shows the net vertical and horizontal forces acting on the wing at stall AOA  $10^\circ$ , and the results indicate that the first configuration at 20% throttle level produced a net vertical force of 6.48N, which did not exceed the baseline clear wing's result of 6.54N. However, the net vertical force increased to 7.33N at 40% throttle level, which is a 12% increase compared to the clear wing's result. This increase in speed is due to the additional propulsive lift generated by the propellers at  $10^\circ$  AOA, as well as the flow acceleration imposed by the propellers. Comparing the four configurations, it was observed that the configuration with propellers placed at 0.71C vertically and 0.33C horizontally from the trailing edge of the wing exhibited the best net vertical force (7.26 N) at 20% throttle (Figure 3.2). At 40% throttle, this configuration had the second highest net vertical force. At 20% throttle, the second-best configuration was the one with the propellers placed at 0.71C vertically and 0.11C horizontally from the trailing edge of the wing. This configuration had the highest net vertical force at 40% throttle (8.04 N) (Figure 3.3). These findings indicate that increasing the throttle percentage leads to an increase in the net vertical force, as illustrated by the higher force measurement at 40% throttle compared to 20%. The observed differences in the maximum net vertical force

between the two configurations may be attributed to changes in the aerodynamic properties of the system.



**Figure 3.1** Net Vertical Force in each Position



**Figure 3.2** Net vertical force at 20% throttle



A comparison of the net vertical force characteristics of the two propeller configurations with 0.22C vertical spacing showed that the configuration with the propellers placed horizontally further (0.33C) from the trailing edge of the wing generated higher net vertical force at both 20% and 40% throttle than the configuration with the propellers placed 0.11C horizontally from the trailing edge of the wing.

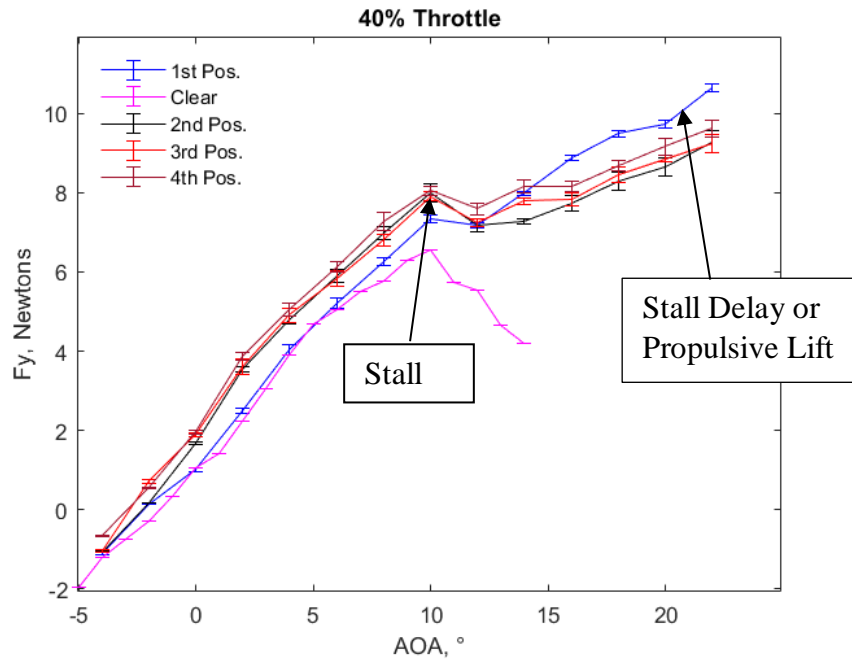


**Figure 3.3** Net vertical force at 40% throttle

In comparison to the other three configurations, the first configuration yields the smallest net vertical force for angles of attack below 14°, as evidenced by the data obtained at both 20% and 40% throttle settings. This can be explained by the Propeller-Wing Interference. The first configuration might have suffered from interference between the propellers and the wing. The proximity of the propellers to the wing could have disrupted the airflow over the wing and led to reduced lift. This effect could be particularly pronounced at low throttle levels where the airflow from the propellers might not be strong enough to overcome the interference effects. Another possible explanation is that the flow from the wing could have affected the performance of the propellers, leading to reduced thrust and efficiency. This effect could be particularly significant for the first and second configurations, where the propellers were located close to the wing. The airflow from the wing could have disrupted the flow around the propellers, leading to turbulent and non-uniform airflow, which could reduce the efficiency and performance of the propellers. This effect could be mitigated by having the propellers located further away from the wing, as in the third and fourth configurations, where the propellers were fully exposed to the flow from above. When the propellers are placed above

the wing, they create an acceleration of the airflow over the upper surface of the wing. This increased airflow velocity results in a reduction of air pressure above the wing, causing a higher-pressure difference between the top and bottom of the wing. This pressure difference generates lift, which helps to keep the wing aloft. Therefore, the placement of the propellers above the wing can increase the lift generated by the wing, which can improve performance of the aircraft. However, the benefit of having the propellers fully exposed to the flow from above could be limited at higher angles of attack, where the propellers might be affected by the turbulent flow over the wing. Hence, from Figure 3.2 and Figure 3.3, it is evident that the first configuration outperforms the remaining three configurations for angles of attack exceeding  $14^\circ$ . Therefore, the performance of the propellers could be influenced by the interaction between the flow from the wing and the flow generated by the propellers, which could vary depending on the location and orientation of the propellers relative to the wing.

#### 4.1.2 Net Horizontal Force

The results indicate that the net horizontal force also varied significantly among the different configurations and throttle settings (Figure 3.5). It is important to note that the minimum horizontal force was found in the second configuration at 40% throttle. The net horizontal force is determined by the difference between the thrust and drag, and if the force is positive, it means that the drag is higher than the thrust generated by the propellers. In all the configurations, the net horizontal force was either positive or slightly below zero.

The second configuration, with the propellers positioned 0.22C vertically and 0.33C horizontally from the trailing edge, resulted in the lowest net horizontal force at both throttle settings. This configuration appears to strike a good balance between the horizontal and vertical distances of the propellers from the trailing edge, minimizing their exposure to the low-pressure region above the wing. The third configuration, with the propellers positioned 0.71C vertically and 0.33C horizontally from the trailing edge, appears to have been affected by the flow from above the wing, since the propellers were entirely above the trailing edge. This configuration resulted in a higher net horizontal force than the second configuration, although it still performed better than the first and fourth configurations.

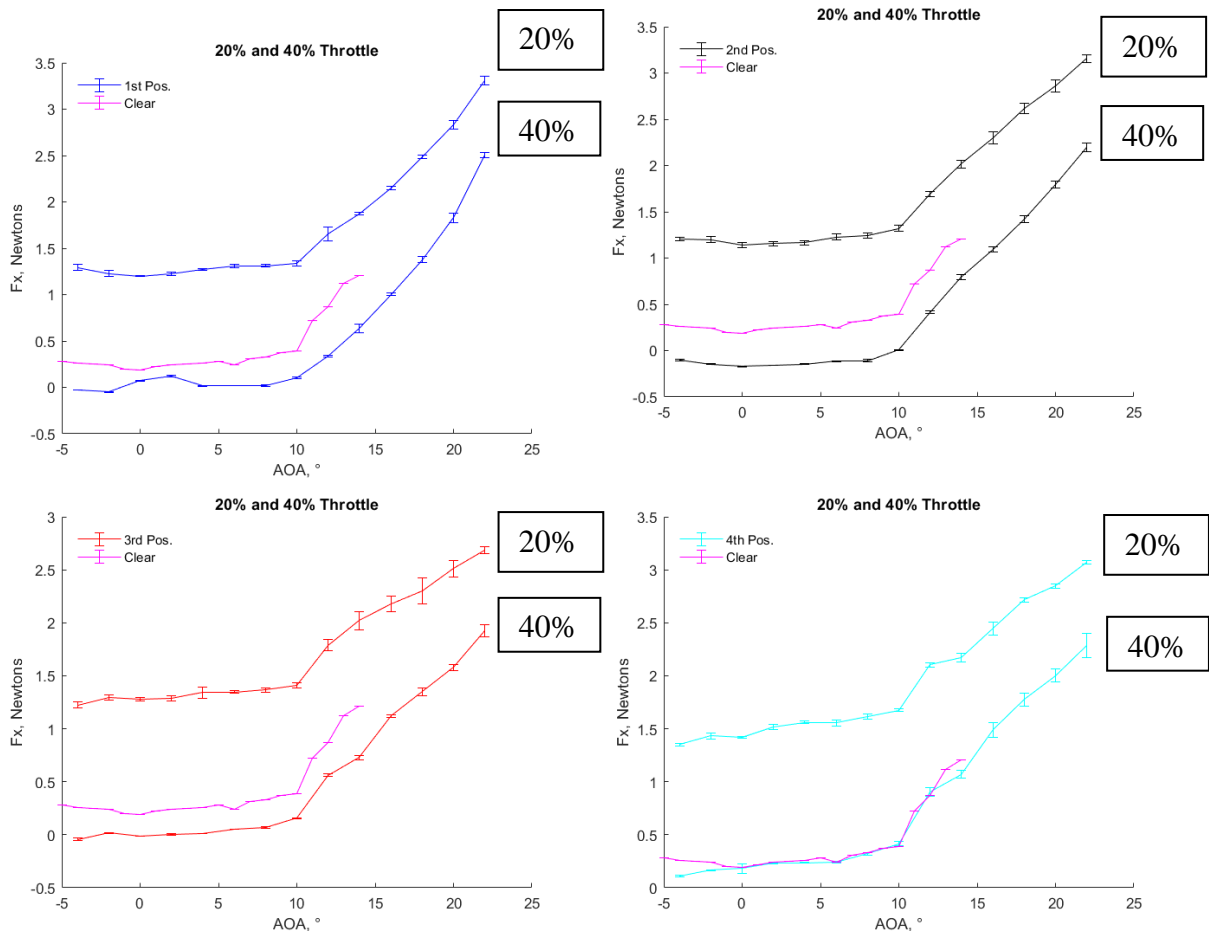


**Figure 3.4** Net Horizontal Force in each Position

The first configuration, with the propellers positioned 0.22C vertically and 0.11C horizontally from the trailing edge, also had a high horizontal force. This may be due to the propellers being positioned close to the wing, which likely deteriorated their performance due to the low-pressure region created by the wing. It is worth noting that the net horizontal force measured includes both drag and thrust forces acting on the wing. While this may affect the interpretation of the results, it is justified in the context of this experiment as the propellers were actively providing thrust to the system.

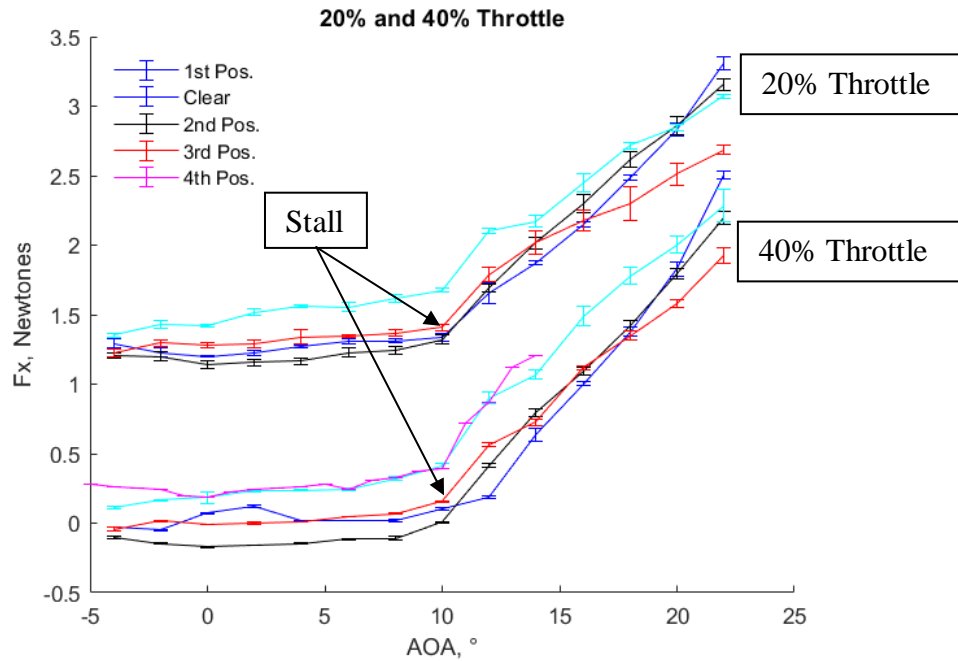


**Figure 3.5** Net horizontal force

## 4.2 Experiment 1: Effect on Lift & Drag

The objective of the experiment was to distinguish the propulsive lift created by propellers, particularly at higher angles of attack, from the lift generated by the wing itself. According to the results, there is an evident indirect impact of the propellers on the wing. Figure 3.6 depicts the lift coefficients at each position. The lift generated by the aircraft was found to be influenced by the propellers, which resulted in an increase in the lift coefficient in all configurations at both 20% and 40% throttle. However, it was observed that the drag coefficient also tended to increase as the throttle was increased (Figure 3.7). This observation makes sense as the increase in throttle leads to a higher flow velocity above the wing, resulting in a higher drag. Before an angle of attack of  $10^\circ$ , the lift coefficient in the first configuration was similar to that of the clear wing. This may be because in the first configuration, the propellers were positioned vertically, aligned with the chord of the wing. This caused the flow to be accelerated not only above the wing but also below it, which did not contribute to the pressure difference as much. By positioning the propellers in this way, the airflow was not optimized to create lift, resulting in minimal aerodynamic effect from the propeller. However, in contrast to the other configurations, the lift coefficient in the first configuration continued to increase rapidly after an angle of attack of  $12^\circ$ .

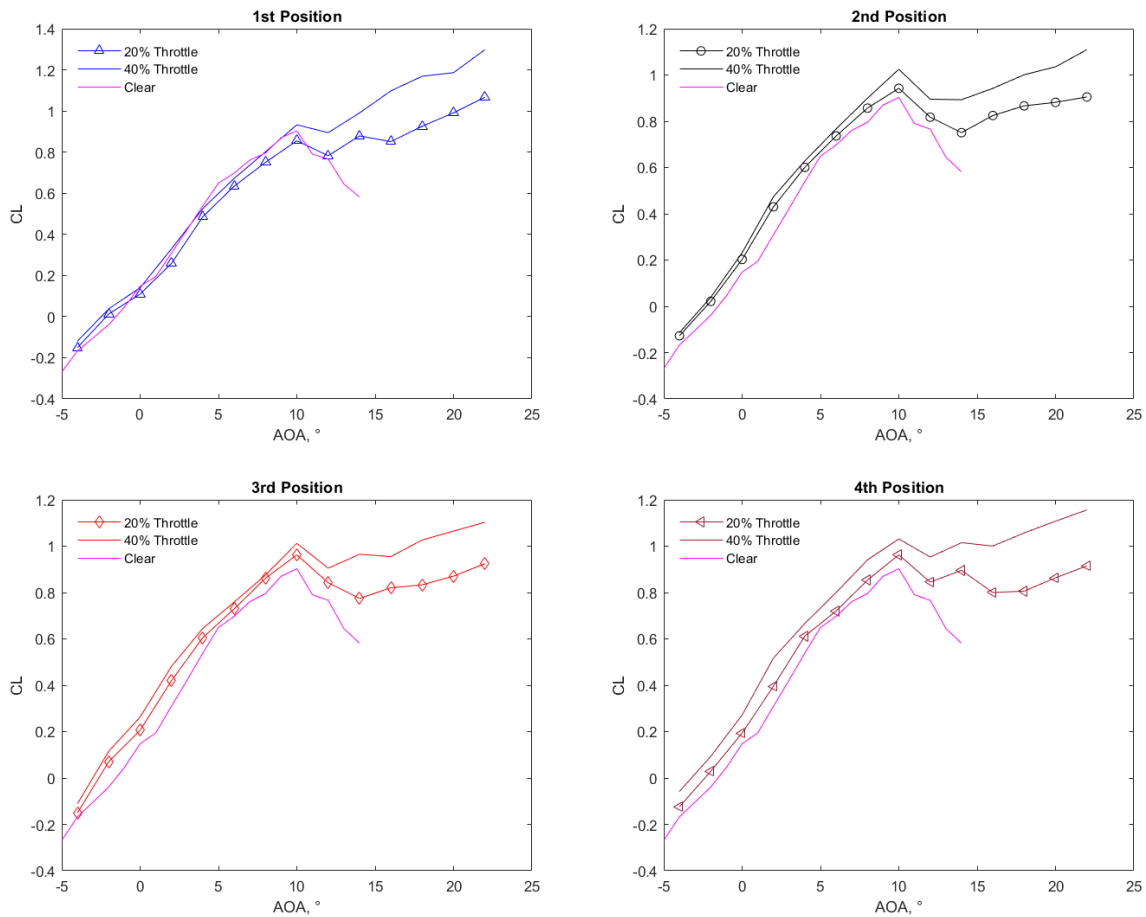


**Figure 3.6** Lift Coefficient in each Position

This may be due to the propellers being positioned closer to the wing in this configuration, which allowed the wing to prevent flow separation at higher angles of attack. The propellers helped to energize the boundary layer and keep the airflow attached to the wing, resulting in increased lift. At smaller angles of attack, the third and fourth configurations outperformed the other two, most likely because the propellers were positioned vertically above the wing surface, resulting in flow acceleration (Figure 3.8). This configuration helped to increase the lift coefficient by energizing the boundary layer of air around the wing. After an angle of attack of  $10^\circ$ , flow separation occurred, and positioning of the propellers did not allow for the airflow to remain attached to the wing. As a result, the lift coefficient decreased, and the performance of these configurations became worse compared to the other two configurations. However, to accurately confirm whether a separation occurred at  $10^\circ$ , it is necessary to perform a Particle Image Velocimetry (PIV) analysis and visually inspect the flow patterns.

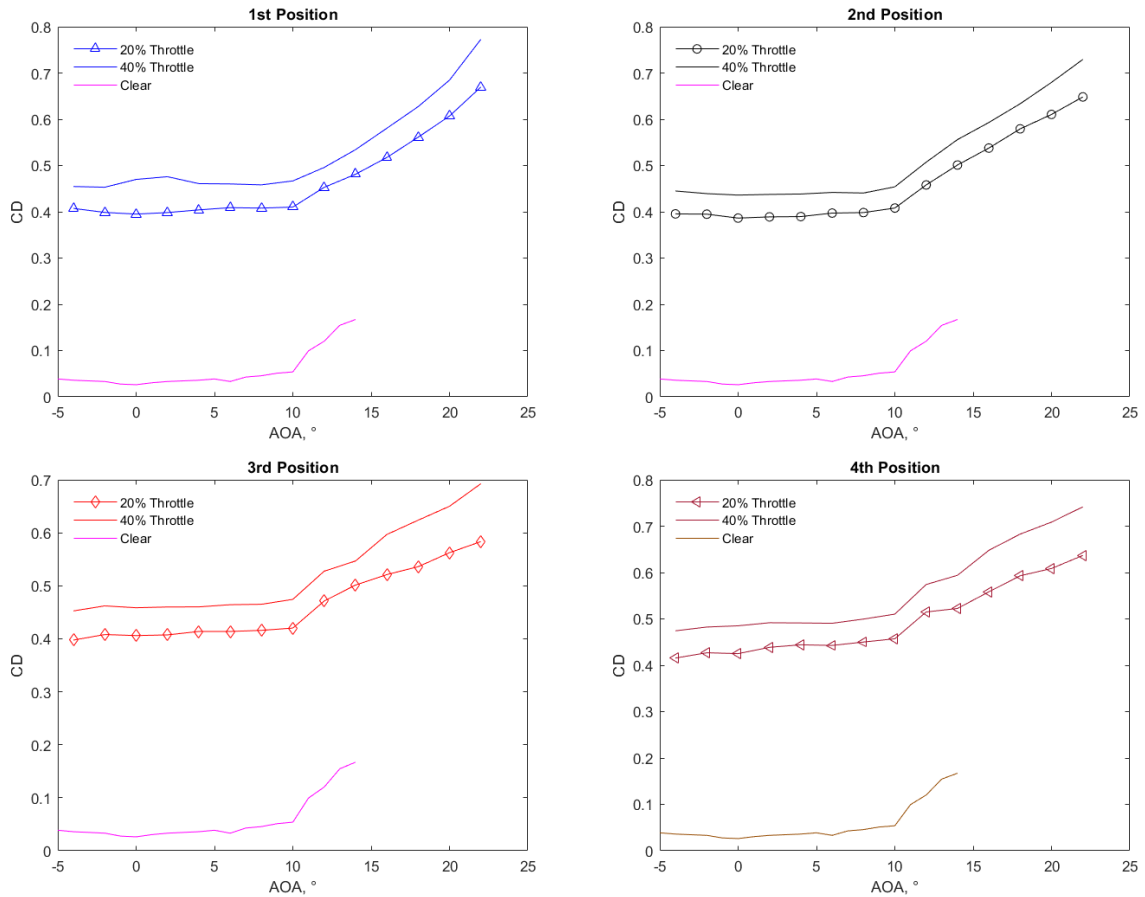


**Figure 3.7 Drag Coefficient in each Position**

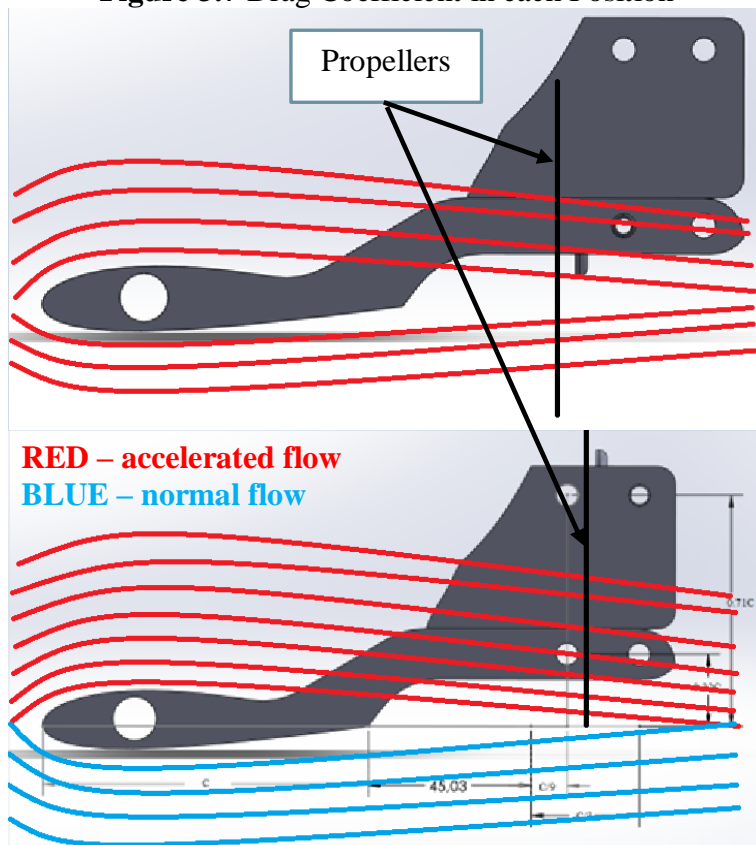


**Figure 3.8 Diagram of flow at 0° AOA (1<sup>st</sup> and 3<sup>rd</sup> configurations, respectively)**

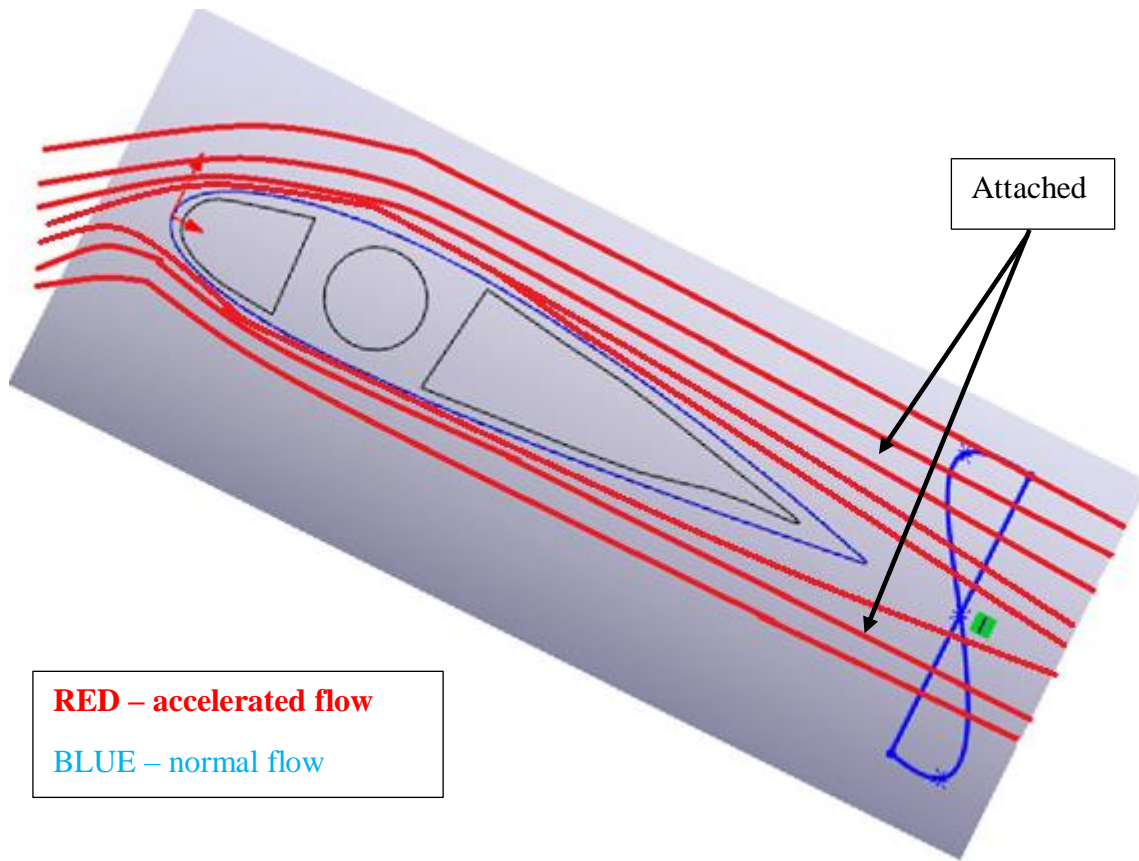


**Figure 3.9** Diagram of flow at higher AOA (1<sup>st</sup> configurations)

### 4.3 Experiment 2: Steady Level Flight

The data obtained from the experiment was analyzed to determine the optimal throttle and freestream velocity for achieving a zero net horizontal and vertical force on the wing (Figure 3.10). The experimental data obtained from the study showed that the lifting force on the wing was approximately 5 N, which is equal to the weight of the wing, indicating that steady level flight conditions had been achieved. The net horizontal force was found to be zero, indicating that the wing was in a steady level flight condition. The data obtained from the experiment was analyzed to determine the optimal throttle and freestream velocity for achieving a zero net horizontal and vertical force on the wing. The results showed that the throttle and freestream velocity for achieving steady level flight conditions varied with angle of attack (Table 3.2).

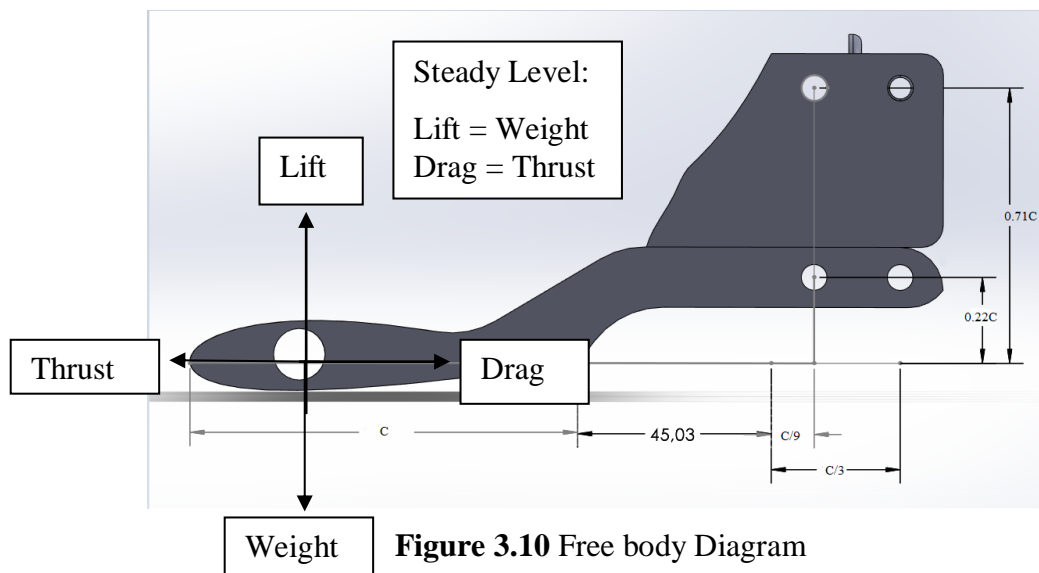
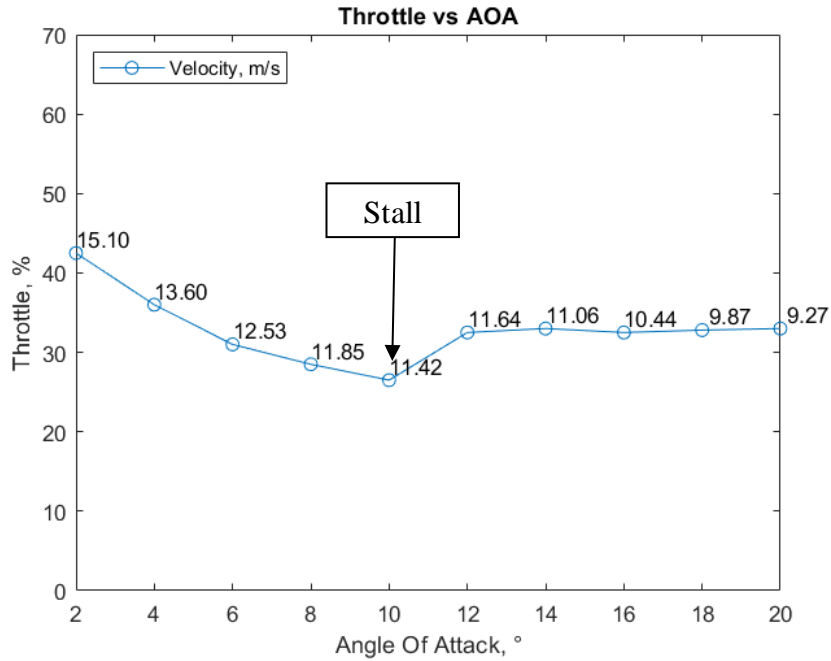


Table 3.2 Trimmed parameters

AOA	Throttle	Velocity, m/s	F <sub>y</sub> , N	F <sub>x</sub> , N
2°	42,5%	15,1	5,05	0,02
4°	36%	13,6	5,02	0
6°	31%	12,5	4,98	0,02
8°	28,5%	11,8	5	0
10°	26,5%	11,4	5,02	0
12°	32,5%	11,6	5,02	0,01
14°	33%	11	4,99	0,01
16°	32,5%	10,4	4,98	0,02
18°	32,8%	9,9	5,05	0,01
20°	33%	9,3	4,98	0,03





**Figure 3.11** Throttle vs AOA

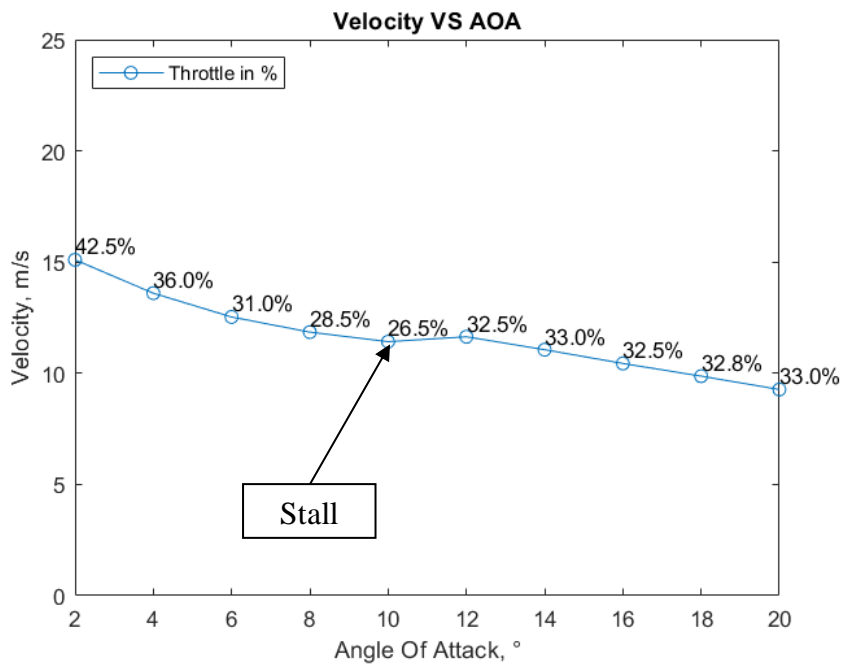


**Figure 3.12** Velocity vs AOA

As the angle of attack (AOA) increases, the required throttle setting decreases (Figure 3.11). For example, at an AOA of 2 degrees, the required throttle setting is 42.5%, while at an AOA of 20 degrees, the required throttle setting is only 33%. This trend suggests that the lift generated by the wing increases as the AOA increases, allowing the aircraft to maintain steady level flight with less power from the propellers. As the AOA increases, the required freestream

velocity decreases (Figure 3.12). For example, at an AOA of 2 degrees, the required freestream velocity is 15.1 m/s, while at an AOA of 20 degrees, the required freestream velocity is only 9.27 m/s. As the AOA increases, the shape of the wing generates more lift, reducing the required freestream velocity to maintain steady level flight.

There is a non-monotonic trend in throttle setting as a function of AOA between 4 and 18 degrees. Specifically, the required throttle setting decreases from 42.5% at 2 degrees to 31% at 6 degrees, then increases to 32.5% at 12 degrees, before decreasing again to 32.8% at 18 degrees. This trend may be due to changes in the balance between lift and drag as the AOA changes. At lower AOAs, increasing the throttle setting generates more lift with relatively little increase in drag, allowing the aircraft to maintain steady level flight with less power. At higher AOAs, increasing the throttle setting generates more drag with relatively little increase in lift, reducing the overall efficiency of the system. The required freestream velocity decreases at a decreasing rate as the AOA increases. This trend suggests that the wing reaches a limit to the amount of lift it can generate as the AOA increases, causing the required freestream velocity to level off. This limit may be due to factors such as stall, where the airflow over the wing becomes turbulent and lift is reduced, or separation, where the airflow over the wing separates from the surface and lift is lost. These trends can help to explain the behavior of the wing with two pusher propellers under different operating conditions and can inform the design and optimization of similar aircraft.

The data shows that lower throttle settings and lower freestream velocities result in lower power consumption, while higher throttle settings and higher freestream velocities provide better lift-to-drag ratios. However, there are trade-offs between these performance metrics, which must be analyzed to determine the optimal operating conditions. For instance, increasing the throttle setting typically leads to higher lift but also increases drag and power consumption. Therefore, to design an efficient system, it is necessary to consider the balance between power consumption and lift generation. By analyzing these trade-offs, a better understanding of the limitations and trade-offs involved in designing and operating a wing with two pusher propellers can be gained. The minimum required throttle level to maintain steady level flight was achieved at 10° AOA, which is consistent with the stall angle observed in the first experiment. At this angle, a throttle level of 26.5% and a freestream velocity of 11.42 m/s were sufficient to maintain the wing's altitude. At 20° AOA, the minimum freestream velocity required for steady level flight was 9.27 m/s, and the throttle level needed to be increased to 33%. After 12° AOA, the freestream velocity began to decrease, likely because the propellers

were generating more vertical lift to compensate for the reduced lift from the wing at higher angles of attack after the stall.

Based on the results of the experiment, it can be concluded that steady level flight is achievable using two pusher propellers at all tested angles of attack (AOA). This indicates that the system is stable and can maintain a consistent flight path under different operating conditions. To optimize the performance of the wing with two pusher propellers, the specific performance metric of interest must be considered.

# Chapter 4 – Conclusion & Future Work

---

*This chapter aims to summarize the work and suggests potential areas for future research to address these shortcomings. Future work could involve expanding the experiments to different conditions and configurations, improving measurement techniques, and refining the theoretical models.*

## 4.1 Conclusion

In summary, this thesis analyzes the performance of a wing with two pusher propellers in four different configurations and provides insights into the effects of propeller positioning and steady level conditions on aerodynamic performance.

Regarding propeller positioning, the results show that the placement of propellers significantly affects the aerodynamic performance of the wing. The first configuration, with propellers positioned close to the wing, resulted in the smallest net vertical force for angles of attack below  $14^\circ$ , possibly due to propeller-wing interference. The second configuration, with propellers positioned  $0.22C$  vertically and  $0.33C$  horizontally from the trailing edge, resulted in the lowest net horizontal force at both throttle settings, striking a good balance between the horizontal and vertical distances of the propellers from the trailing edge. The third and fourth configurations, which exposed the propellers fully to the flow from above, produced greater net vertical and horizontal forces. However, in the fourth configuration, the drag force was greater than the thrust generated by the propellers, resulting in a higher net horizontal force.

When it comes to the lift and drag, the results showed that the propellers indirectly impacted the lift coefficient, increasing it in all configurations at both throttle positions. The drag coefficient tended to increase as throttle increased, leading to higher flow velocity and higher drag. The position of propellers influenced the lift coefficient, with the first configuration having minimal aerodynamic effect and the third and fourth configurations outperforming the other two at smaller angles of attack. However, after an angle of attack of  $10^\circ$ , flow separation occurred, and the performance of these configurations became worse.

Regarding steady level conditions, the data shows that lower throttle settings and lower freestream velocities result in lower power consumption, while higher throttle settings and higher freestream velocities provide better lift-to-drag ratios. The minimum required throttle level to maintain steady level flight was achieved at  $10^\circ$  AOA, which is consistent with the stall angle observed in the first experiment. At  $20^\circ$  AOA, the minimum freestream velocity required for steady level flight was  $9.27$  m/s, and the throttle level needed to be increased to

33%. After 10° AOA, the freestream velocity began to decrease, indicating a reduction in lift generation by wing and compensating it by the propulsive lift generated by the propellers.

The findings of the report can be used to optimize the placement of propellers for maximum performance in the design and development of aircraft with similar configurations, and to understand the trade-offs between power consumption and lift generation in steady level flight.

## 4.2 Limitations

This study has some limitations that should be considered. First, the experiment was conducted in a wind tunnel, which may not completely simulate the actual flight conditions. The wind tunnel does not consider the effect of the surrounding air, which could affect the lift and drag characteristics of the wing. Additionally, the wing's airfoil and geometry were not optimized for the propeller configuration, which could have affected the performance of the wing. Further studies could investigate the effect of different wing designs and airfoils on the lift and drag characteristics of the wing with two propellers.

## 4.3 Future Work

Future work could involve testing different wing designs and airfoils to determine the effect of these factors on the lift and drag characteristics of a wing with two propellers placed behind it. Additionally, experiments could be conducted at different operating conditions, such as different propeller speeds or angles of attack, to investigate the effect of these factors on the aerodynamic performance of the wing. Another area for future research could involve the impact of propeller placement on the noise level generated by the aircraft. Noise pollution is a significant issue for the aviation industry, and the placement of propellers could potentially affect the amount of noise generated by the aircraft. Thus, future studies could investigate the impact of different propeller configurations on noise levels and explore methods for reducing the noise generated by the aircraft. In addition to experimental studies, computational simulations could also be used to investigate the aerodynamic performance of wing models with different propeller configurations. Computational fluid dynamics (CFD) simulations could provide a more detailed understanding of the airflow around the wing and propellers, enabling researchers to identify areas of flow separation or turbulence that could be affecting the performance of the wing. Finally, the findings of this study could be used to inform the design and development of aircraft with similar configurations. The optimal placement of propellers identified in this study could be used as a starting point for the design of new aircraft,

with further modifications and optimizations made based on the specific requirements of the aircraft. Ultimately, the results of this study contribute to a better understanding of the complex interactions between wings and propellers and could help to improve the performance and efficiency of aircraft in the future.

## References

- [1] [“Aviation Sustainability: Facts and Figures,” *Green Baggage*. <https://www.greenbaggage.org/news-and-media/aviation-sustainability-facts-and-figures> (accessed Dec. 18, 2022).
- [2] M. Tahir, S. Ahmed Khan, T. Khan, M. Waseem, D. Khan, and A. Annuk, “More electric aircraft challenges: A study on 270 V/90 V interleaved bidirectional DC–DC converter,” *Energy Reports*, vol. 8, pp. 1133–1140, Nov. 2022, doi: 10.1016/j.egy.2022.06.084.
- [3] P. Okonkwo and H. Smith, “Review of evolving trends in blended wing body aircraft design,” *Progress in Aerospace Sciences*, vol. 82, pp. 1–23, Apr. 2016, doi: 10.1016/j.paerosci.2015.12.002.
- [4] “X-48B Blended Wing Body,” *NASA*. <http://www.nasa.gov/centers/dryden/research/X-48B/index.html> (accessed Dec. 18, 2022).
- [5] “N3-X - Glenn Research Center | NASA,” *Glenn Research Center | NASA*. <https://www1.grc.nasa.gov/aeronautics/eap/airplane-concepts/n3x/> (accessed Dec. 18, 2022).
- [6] M. T. Fard, J. He, H. Huang, and Y. Cao, “Aircraft Distributed Electric Propulsion Technologies—A Review,” *IEEE Transactions on Transportation Electrification*, vol. 8, no. 4, pp. 4067–4090, Dec. 2022, doi: 10.1109/tte.2022.3197332.
- [7] A. S. Gohardani, “A synergistic glance at the prospects of distributed propulsion technology and the electric aircraft concept for future unmanned air vehicles and commercial/military aviation,” *Progress in Aerospace Sciences*, vol. 57, pp. 25–70, Feb. 2013, doi: 10.1016/j.paerosci.2012.08.001.
- [8] P. F. Pelz, P. Leise, and M. Meck, “Sustainable aircraft design — A review on optimization methods for electric propulsion with derived optimal number of propulsors,” *Progress in Aerospace Sciences*, vol. 123, p. 100714, May 2021, doi: 10.1016/j.paerosci.2021.100714.

- [9] L. Menegozzo and E. Benini, “Boundary Layer Ingestion Propulsion: A Review on Numerical Modeling,” *Journal of Engineering for Gas Turbines and Power*, vol. 142, no. 12, Dec. 2020, doi: 10.1115/1.4048174.
- [10] P. F. Pelz, P. Leise, and M. Meck, “Sustainable aircraft design — A review on optimization methods for electric propulsion with derived optimal number of propulsors,” *Progress in Aerospace Sciences*, vol. 123, p. 100714, May 2021, doi: 10.1016/j.paerosci.2021.100714.
- [11] “X-57 Maxwell,” *X-57 Maxwell*. <https://www.nasa.gov/specials/X57> (accessed Dec. 18, 2022).
- [12] E. Dillinger et al., “Handling qualities of ONERA’s small business concept plane with distributed electric propulsion,” in Proc. 31st Congr. Int. Council Aeronaut. Sci., 2018, pp. 1–10.
- [13] X.-G. Yang, T. Liu, S. Ge, E. Rountree, and C.-Y. Wang, “Challenges and key requirements of batteries for electric vertical takeoff and landing aircraft,” *Joule*, vol. 5, no. 7, pp. 1644–1659, Jul. 2021, doi: 10.1016/j.joule.2021.05.001.
- [14] “Vahana,” *Vahana Airbus*, Jul. 01, 2021. <https://www.airbus.com/en/urbanairmobility/cityairbus-nextgen/vahana> (accessed Dec. 18, 2022).
- [15] J. D. Anderson, *Fundamentals of Aerodynamics*. 2016.
- [16] M. E. El-Salamony and L. L. Teperin, “Parametric Studies on Airfoil-Boundary Layer Ingestion Propulsion System,” *SAE International Journal of Aerospace*, vol. 13, no. 1, pp. 43–55, Mar. 2020, doi: 10.4271/01-13-01-0003.
- [17] M. H. SNYDER and G. W. ZUMWALT, “Effects of wingtip-mounted propellers on wing lift and induced drag.,” *Journal of Aircraft*, vol. 6, no. 5, pp. 392–397, Sep. 1969, doi: 10.2514/3.44076.
- [18] J. LOTH and F. LOTH, “Induced drag reduction with wing tip mounted propellers,” *2nd Applied Aerodynamics Conference*, Aug. 1984, **Published**, doi: 10.2514/6.1984-2149.



- [19] L. MIRANDA and J. BRENNAN, “Aerodynamic effects of wingtip-mounted propellers and turbines,” *4th Applied Aerodynamics Conference*, Jun. 1986, **Published**, doi: 10.2514/6.1986-1802.
- [20] “Piaggio P.180 Avanti — Wikimedia Commons,” *Piaggio P.180 Avanti — Wikimedia Commons*.  
[https://commons.wikimedia.org/w/index.php?title=Piaggio\\_P.180\\_Avanti&uselang=uk](https://commons.wikimedia.org/w/index.php?title=Piaggio_P.180_Avanti&uselang=uk)  
 (accessed Dec. 18, 2022).
- [21] D. P. Raymer, *Aircraft Design: a Conceptual Approach*. 2018.
- [22] J. Roskam, *Preliminary configuration design and integration of the propulsion system*. Lawrence, Kan: DARcorporation, 2004.
- [23] P. W. Brown, “Flight test results for several light, Canard-configured airplanes,” *SAE Technical Paper Series*, 1987.
- [24] “ASK DJ Aerotech Question,” *ASK DJ Aerotech Question*.  
[https://web.archive.org/web/20111121020132/http://djaerotech.com/dj\\_askjd/dj\\_questions/propeffects.html](https://web.archive.org/web/20111121020132/http://djaerotech.com/dj_askjd/dj_questions/propeffects.html) (accessed Dec. 18, 2022).
- [25] B. Li, H. Lu, and S. Deng, “Validation of an actuator disk model for numerical simulation of propeller,” *Proceedings of the Institution of Mechanical Engineers, Part G: Journal of Aerospace Engineering*, vol. 229, no. 8, pp. 1454–1463, Oct. 2014, doi: 10.1177/0954410014553488.
- [26] S. Zhao and D. Xu, “Effects of distributed propellers slipstream on aerodynamic characteristics of Wing,” *Lecture Notes in Electrical Engineering*, pp. 255–267, 2019.
- [27] J. R. Serrano, A. O. Tiseira, L. M. García-Cuevas, and P. Varela, “Computational Study of the Propeller Position Effects in Wing-Mounted, Distributed Electric Propulsion with Boundary Layer Ingestion in a 25 kg Remotely Piloted Aircraft,” *Drones*, vol. 5, no. 3, p. 56, Jun. 2021, doi: 10.3390/drones5030056.
- [28] Y. Ma, W. Zhang, Y. Zhang, K. Li, and Y. Wang, “Effects of distributed propulsion crucial variables on aerodynamic and propulsive performance of small UAV,” *Lecture Notes in Electrical Engineering*, pp. 1535–1550, 2019.

- [29] X. ZHANG, W. ZHANG, W. LI, X. ZHANG, and T. LEI, “Experimental research on aero-propulsion coupling characteristics of a distributed electric propulsion aircraft,” *Chinese Journal of Aeronautics*, Jul. 2022, Published, doi: 10.1016/j.cja.2022.07.024.
- [30] L. W. Khang, “An Investigation on the effects of Distributed Propulsion System on Aerodynamic Performance of a Fixed Wing,” *Proceedings of the URECA@NTU*, 2021.
- [31] R. de Vries, N. van Arnhem, T. Sinnige, R. Vos, and L. L. M. Veldhuis, “Aerodynamic interaction between propellers of a distributed-propulsion system in forward flight,” *Aerospace Science and Technology*, vol. 118, p. 107009, Nov. 2021, doi: 10.1016/j.ast.2021.107009.
- [32] S. Mikhalyov, A. Dunaevsky, L. Teperin, R. Vasilyev, and A. Redkin, “Effects of Propeller Slipstream of Distributed Electric Propulsion on the Wing-Flap System,” *MATEC Web of Conferences*, vol. 304, p. 02018, 2019, doi: 10.1051/mateconf/201930402018.
- [33] W. Zhao, Y. Zhang, P. Tang, and J. Wu, “The Impact of Distributed Propulsion on the Aerodynamic Characteristics of a Blended-Wing-Body Aircraft,” *Aerospace*, vol. 9, no. 11, p. 704, Nov. 2022, doi: 10.3390/aerospace9110704.
- [34] N. Corporation., “Nidec Corporation,” *Nidec Corporation*. <https://www.nidec.com/en/technology/motor/glossary/000/0609/> (accessed Dec. 19, 2022).

# Appendix A

## Arduino code

```
#include <Servo.h>

byte servoPin = 9; %Connect Motor 1 Signal to pin 9 (Digital PWM)
byte servoPin1 = 8; %Connect Motor 2 Signal to pin 8 (Digital PWM)
Servo servo;
Servo servo1;

void setup() {

  Serial.begin(9600);
  servo.attach(servoPin);
  servo1.attach(servoPin1);

  servo.writeMicroseconds(1000); // Initialize the ESC controller, mid-point at
1000 PWM
  servo1.writeMicroseconds(1000);

  delay(7000); // delay to allow the ESC to recognize the stopped signal
}

void loop() {

  Serial.println("Enter PWM signal value 1100 to 1800, 1000 to stop");

  while (Serial.available() == 0);

  int val = Serial.parseInt();

  servo.writeMicroseconds(val); // Send signal to ESC.
  servo1.writeMicroseconds(val); //Send signal to ESC1
}
```

